A TRAJECTORY STUDY OF THE SEASONAL CYCLE OF THE TROPICAL LOWER STRATOSPHERIC WATER VAPOR IN CHEMISTRY-CLIMATE MODELS IN COMPARISON WITH OBSERVATIONS

A Thesis

by

XUN WANG

Submitted to the Office of Graduate and Professional Studies of
Texas A&M University
in partial fulfillment of the requirement for the degree of

MASTER OF SCIENCE

Chair of Committee,	Andrew E. Dessler
Committee Members,	John W. Nielsen-Gammon
	Gerald R. North
Head of Department,	Ping Yang

August 2017

Major Subject: Atmospheric Sciences

ABSTRACT

In this study, we evaluate how well the Goddard Earth Observing System Chemistry Climate Model (GEOSCCM) and the Whole Atmosphere Community Climate Model (WACCM) reproduce the seasonal cycle of the tropical lower stratospheric water vapor in the Microwave Limb Sounder (MLS) and the European Centre for Medium-Range Weather Forecasts (ECMWF) ERA-Interim (ERAi). We also evaluate how well the chemistry-climate models (CCMs) reproduce the key processes that regulate the seasonal cycle using a forward, domain filling, diabatic trajectory model. The seasonal cycle from the MLS, the ERAi, and the CCMs show general agreement. The troposphere-to-stratosphere transport of water vapor in the trajectory model driven by the GEOSCCM (traj-GEOSCCM) and the trajectory model driven by the WACCM (traj-WACCM) show differences when compared to the trajectory model driven by the ERAi (traj-ERAi). The traj-GEOSCCM underestimates the contribution to stratospheric water vapor from the Asian monsoon region during summer, while the traj-WACCM run overestimates the contribution to stratospheric water vapor from the Tropical West Pacific throughout the year. The final dehydration point (FDP) of parcels in the traj-ERAi run is well reproduced in the GEOSCCM run. The traj-WACCM run, however, overestimates the FDP density in the Tropical West Pacific and underestimates it in Tropical Africa and South America. The traj-WACCM run also shows a higher average FDP altitude. Both the traj-GEOSCCM and traj-WACCM do a good job reproducing the contribution to the seasonal oscillation of the tropical lower stratospheric water vapor in the traj-ERAi. Finally, both the CCMs predict that the seasonal cycle will be

moister throughout the year by the end of the 21st century. The mean of the seasonal cycle increases by 0.93 ppmv (25%) in the GEOSCCM and 1.85 ppmv (41%) in the WACCM. The amplitude of the seasonal cycle in the GEOSCCM is predicted to increase by 0.64 ppmv (36%), while that in the WACCM will decrease by 0.32 ppmv (28%). The trajectory model driven by the two CCMs underpredict the changes in the moisture and amplitude of the seasonal cycle from the CCMs.

CONTRIBUTORS AND FUNDING SOURCES

Contributors

This work was supervised by a thesis committee consisting of Dr. Andrew E. Dessler, Dr. John W. Nielsen-Gammon and Dr. Gerald R. North of the Department of Atmospheric Sciences, Texas A&M University.

The GEOSCCM data for analyses in Chapter III was provided by Dr. Luke Oman of NASA Goddard Space Flight Center. The WACCM for analyses in Chapter III was provided by Dr. Karen Rosenlof of NOAA Earth Science Research Laboratory. The input data for trajectory analysis in Chapter III was processed by Hao Ye of the Department of Atmospheric Sciences, Texas A&M University.

All other work conducted for the thesis was completed by the student independently.

Funding sources

Graduate study was supported by NASA grant NNX14AF15G to Texas A&M University.

ACKNOWLEDGMENTS

I would like to thank my advisor, Dr. Andrew Dessler. With his support and instructions, my graduate-student life at the Department of Atmospheric Sciences, Texas A&M has been worthy and rewarding. I also wish to thank my committee members Dr. John Nielsen-Gammon and Dr. Gerald North for providing inspiring suggestions while I work on my thesis. Great appreciation also goes to Dr. Mark Schoeberl, Dr. Kenneth Bowman, and Dr. Tao Wang, who, along with Dr. Andrew Dessler, developed the trajectory model I used in this study. In addition, many thanks to Dr. Ping Yang for inviting me and other fellow group members to take part in the joint-group meetings.

Besides, I would like to thank my group members and colleagues in the Department of Atmospheric Sciences at Texas A&M, who have offered me all kinds of help and have made my graduate-student life pleasant and cheerful, which is of great importance. Special thanks to Wandi Yu, Hao Ye, and Kevin Smalley for their inspiring discussions with me and their technical help. I'd also like to thank the Geosiences IT staff, Brady Dennis, Theresa Morrison, Irene Martinez, Diana Mills and other staff at the Department of Atmospheric Sciences, Texas A&M for offering me all kinds of help including help on IT issues, academic, and finical issues while I study and work here.

Finally, great thanks to my parents and my friends for their love and support.

NOMENCLATURE

BDC	Brewer-Dobson circulation
CCM	chemistry-climate model
DJF	December-January-February (boreal winter)
ECMWF	European Centre for Medium-Range Weather Forecasts
ERAi	ERA-Interim
FDP	final dehydration point
GEOSCCM	Goddard Earth Observing System Chemistry Climate Model
H_2O	water vapor
JJA	June-July-August (boreal summer)
RCP	Representative Concentration Pathway
TST	trosposphere-to-stratosphere transport
TTL	tropical tropopause layer
WACCM	Whole Atmosphere Community Climate Model

TABLE OF CONTENTS

LIST OF FIGURES

LIST OF TABLES

I INTRODUCTION

I.1 Stratospheric water vapor

Stratospheric water vapor is important in stratospheric chemistry because it is the major source of hydroxyl (OH) radicals, which play a role in regulation of ozone [Solomon et al., 1986]. Stratospheric water vapor also affects the radiative budget of the atmosphere: Both observations and model simulations show increases in stratosphere humidity cool the stratosphere and warm the troposphere [e.g. Forster and Shine, 1999; Dvortsov and Solomon, 2001; Shindell, 2001; Forster and Shine, 2002; Solomon et al., 2010]. Atmospheric GCM simulations also show that the changes in stratospheric temperatures resulting from stratospheric water vapor trends may also influence stratospheric circulation [Maycock et al., 2013]. Moreover, warming of the climate system may lead to moistening of the stratosphere, thereby generating a potential stratospheric water vapor feedback [Dessler et al., 2013]. Therefore, the scientific community has attached great importance to improving out understanding of the processes that control stratospheric water vapor.

I.2 The source of stratospheric water vapor

Water vapor in the stratosphere comes from two major sources: oxidation from methane in upper stratosphere [e.g. Bates and Nicolet, 1950; Dessler et al., 1994] and direct troposphere-to-stratosphere transport (TST). TST occurs when air is transported from upper troposphere to lower stratosphere by the wave driven Brewer-Dobson circulation

(BDC) or occasionally by small-scale convective overshooting directly from the boundary layer in the deep tropics [Fueglistaler et al., 2009].

It has become clear over the years that, in the tropics, the transition from troposphere to stratosphere does not happen sharply, but happens gradually between 355 K (150 hPa, 14 km) and 425 K ($\sim$ 70 hPa, 18.5 km) potential temperature in the tropics. This region shares both the tropospheric and stratospheric properties and is often referred to as the "tropical tropopause layer" (TTL) [Sherwood and Dessler, 2000; Fueglistaler et al., 2009]. Essential dehydration takes place during the slow ascent through the TTL [Sherwood and Dessler, 2000; Fueglistaler et al., 2009], and it largely determines the budget of stratospheric water vapor [Mote et al., 1996; Randel et al., 2004; Fueglistaler et al., 2005].

There have been extensive studies on what controls the stratospheric water vapor during the slow ascent through the TTL, and much progress has been made. To explain the low concentration of moisture in the stratosphere, Brewer [1949] noted that most air enters the stratosphere above the deep tropics, where it encounters extremely low tropical tropopause temperatures and most of the water condenses and is removed. Then air is transported poleward to mid-latitudes and downward at higher latitudes. Newell and Gould-Stewart [1981] postulated a "stratospheric fountain" to add more detail to the theory and to explain the low stratospheric water vapor concentrations compared to the tropical tropopause temperatures. They suggested that air enters the stratosphere through regions with lowest temperatures in the tropical Western Pacific. Later Dessler [1998] re-examined the "stratospheric fountain" and found that the theory of air entering the stratosphere pref-

erentially in colder regions may not be necessary since the annually and zonally averaged water vapor mixing ratio entering the stratosphere agrees with the tropical-tropopause minimum saturation. Holton and Gettelman [2001] pointed out the horizontal transport of air during the slow ascent may explain the discrepancy between the average tropopause temperature and the observed low concentration of water vapor. They suggested that, while traveling upward, moist air may go through the ”cold trap” following horizontal advection, rather than following direct vertical motions, so that it is these coldest temperatures that determine the moisture of air entering the stratosphere.

Since tropical tropopause temperature largely controls stratospheric water vapor, the strong seasonal cycle in the tropical tropopause temperature is imprinted on the annual cycle of the tropical lower stratospheric water vapor [Mote et al., 1995, 1996]. This signal is commonly referred to as stratospheric water vapor tape recorder. Later observations pointed out that the seasonal cycle of the stratospheric water vapor is not spatially uniform. Early analyses based on satellite measurements suggested that the seasonal cycle of water vapor at 100 hPa has maxima in the northern hemisphere subtropics, and that both stratospheric moist and dry air are transported from the northern hemisphere tropics to the deep tropics and southern hemisphere [Randel et al., 1998; Pumphrey et al., 2000]. Other observational studies on the seasonal variation of water vapor pointed out the largest seasonal cycle was observed near northern hemisphere monsoon regions, which were emphasized as the source regions for the seasonal cycle [e.g. Randel et al., 2001; Park et al., 2004]. The spatial variations of the seasonal cycle suggest that the mechanisms that control the

concentration of stratospheric water vapor are complicated, so it is necessary to enhance the understanding of the source of the stratospheric water vapor.

Further details concerning the transport pattern and dehydration locations in the TTL have been explored with the aid of Lagrangian trajectory models, which have been able to accurately simulate water vapor concentrations in the TTL and lower stratosphere [e.g. Gettelman et al., 2002; Jensen and Pfister, 2004; Fueglistaler et al., 2005; Schoeberl and Dessler, 2011]. Trajectory studies have shown that the initialization location of most air parcels that make it to the stratosphere lies in the Tropical West Pacific at the base of the TTL, and that most air parcels in the TTL are transported through the Tropical West Pacific and dehydrate there, following the upper level horizontal circulation during slow ascent [Hatsushika and Yamazaki, 2003; Fueglistaler et al., 2004;Schoeberl et al., 2013]. By comparing the impact of different hypothetical transport pathways on the predicted water vapor, Bonazzola and Haynes [2004] confirmed that the pattern of both vertical transport and horizontal transport are important in determining the budget of the stratospheric water vapor. Levine et al. [2007], using both a tracer transport model and trajectory calculations, also suggested that although in winter most stratospheric tracers originated from the Tropical West Pacific, their vertical motion through the TTL is accompanied by horizontal transport, and that they entered the stratosphere in many locations.

Meanwhile, previous studies have also focused on the South-East Asian monsoon region, where the transport pathway has been well explored, but the impact from that region on the mean tropical stratospheric water vapor is still being debated. Early global

model simulations suggested the primary source for moisture in the tape recorder signal is the air stream originating from the South-East Asian monsoon [Bannister et al., 2004; Gettelman et al., 2004; Lelieveld et al., 2007]. Trajectories initialized within the Asian summer monsoon anticyclone suggested that air is lofted from the planetary boundary layer by convection into the anticyclone, where it is organized in the upper troposphere and is transported further upward into the stratosphere following the strong upwelling [Bergman et al., 2013; Garny and Randel, 2016]. Orbe et al. [2015] investigated the air mass origin from boundary layer using tracer independent model calculations, and concluded that 20% of the tropical lower stratospheric air originated from Asia. However, Wright et al. [2011] showed that even though in boreal summer Southeast Asia is an important region of origin for lower stratospheric air, its contribution to the tropical mean stratospheric water vapor during the annual maximum is small. Schoeberl et al. [2013] also suggested that although there's isolation of the air during TST in the Asian monsoon region, it is not contributing as much as the deep tropics.

I.3 The stratospheric water vapor in a changing climate

Understanding how stratospheric water vapor will change during the 21st century is of great importance to the modeling community, since the changes have important impacts on the climate [e.g. Forster and Shine, 1999; Maycock et al., 2013; Dessler et al., 2013]. Previous studies have mostly focused on the trend of the stratospheric water vapor in the climate models. Gettelman et al. [2010] analyzed 18 coupled chemistry-climate models

and showed that water vapor above the tropical tropopause is predicted to increase during the 21st century. Meanwhile, several studies suggested qualitatively that the long-term changes in the stratospheric water vapor are in agreement with the trend of the temperatures in the TTL [e.g. Fueglistaler and Haynes, 2005; Oman et al., 2008; Gettelman et al., 2009; Kim et al., 2013]. Dessler et al. [2016] showed that, in two chemistry-climate models, 50-80% of the increase in tropical lower stratosphere humidity is attributed to the warming trend of the TTL, and that the remainder of the increase can be explained by the trend in the evaporation of ice lofting from convective overshooting.

Since the seasonal cycle is one of the key features of the tropical lower-stratospheric water vapor, it is important to understand how the seasonal cycle will change in a warming climate. Smith et al. [2000] investigated the trends in the seasonality from January 1992 to April 1999 using HALOE water vapor data and pointed out that there's an increasing trend in the amplitude above the tropical tropopause. However, there's a lack of studies examining how the seasonal cycle of the tropical lower stratospheric water vapor will change as the climate changes during the 21st century in climate models.

I.4 Motivation and thesis outline

We infer from previous studies that the seasonal cycle is one of the key features of the tropical lower stratospheric water vapor, so it is important that the climate models reproduce the observed seasonal cycle. Since the previous studies showed that small variations in the transport and dehydration of moisture in the TTL may lead to important changes in

many aspects of the stratospheric water vapor, it is also important that the good simulations of the tropical lower stratospheric water vapor in the climate models come from good simulations of the key processes that regulate the water vapor. Also, there's a lack of studies investigating how the seasonal cycle of the tropical lower stratospheric water vapor will change during the 21st century in the climate models, so it is interesting to explore it and relate the changes in the seasonal cycle with the changes in the key processes that regulate it.

In our study, we explore how well two state-of-the-art chemistry-climate models (CCMs) reproduce the seasonal cycle of the tropical lower stratospheric water vapor by comparing the seasonal cycle from the CCMs to that from the observations and reanalyses. We also examine the large-scale transport and dehydration in the TTL in a Lagrangian forward trajectory model driven by the CCMs and reanalysis meteorological fields. In particular, we will answer these following questions:

1) How well do the CCMs reproduce the tropical lower stratospheric water vapor, especially its seasonal cycle?

2) If the CCMs do reproduce the seasonal cycle accurately, does that come from their good simulations in the key processes that regulate the tropical lower stratospheric water vapor? Or if they don't well reproduce the seasonal cycle, what can be missing in the key processes? We address this question using the trajectory model driven by the CCMs in three aspects: the details of the transport of water vapor into the stratosphere, the final dehydration locations of air parcels, and the regional contribution to the seasonal cycle.

3) How does the seasonal cycle of the tropical lower stratospheric water vapor change during the 21st century in the CCMs, and can the trajectory model driven by the CCMs reproduce those changes?

4) How do the final dehydration locations change during the 21st century in the trajectory model driven by the CCMs?

II METHODS

II.1 Trajectory model setup

We use the forward, domain filling, diabatic trajectory model described in Schoeberl and Dessler [2011] in this study. The model uses the Bowman trajectory code [Bowman, 1993; Bowman and Carrie, 2002] and is driven by 6-hourly heating rate and two dimensional horizontal winds from reanalyses or chemistry-climate models (CCMs). The trajectory model integration begins with parcels initialized in the upper troposphere on an equal area longitude-latitude grid which is approximately 5° by 5°, and covers 0-360° longitude and $\pm$ 40° latitude. The initialization level is 360 K potential temperature, which is above the average level of zero heating ($\sim$ 355-360 K) [Fueglistaler et al., 2009] but below the tropical tropopause, so that most parcels move upward following the ascending branch of the BDC and experience dehydration.

All parcels are initialized with 200 parts per million by volume (ppmv) H_2O. The trajectory model's time step is 45 minutes and uses a standard fourth-order Runge-Kutta scheme. At the end of each day, any parcel that moves above 5000 K or below 250 hPa is removed. Reanalysis or CCM temperatures are linearly time-space interpolated to parcel locations to determine the local relative humidity (RH) along each trajectory. Anytime the RH exceeds 100%, which is the predetermined saturation threshold, parcels are dehydrated so that RH is reduced to the saturation threshold. We define a parcel to have reached the final dehydration point (FDP) if no further dehydration occurs in 180 days. Finally, methane

oxidation is included in the model, but is unimportant in the region of the atmosphere we are focusing on. We do not include adjustments for missing cloud physics or unresolved temperature fluctuations, which could lead to lower or higher simulated water vapor concentrations than observations [Schoeberl et al., 2014; Schoeberl et al., 2015], but has little impact on anomalies (deviations from a reference state).

We will first analyze the period 2005 to 2014 based on data from the reanalysis and the CCMs. Parcels are injected every day for two consecutive years (i.e. 2004 - 2005, 2006 - 2007, ..., 2013 - 2014), and each trajectory is integrated to the end of the second year. We analyze the second year of each two-year period (i.e. 2005, 2006, ..., 2014), because the stratospheric domain is filled during the second year. All results shown are the mean of the ten-year analyses. Then we repeat the test for the period 2089 to 2098 based on data just from the CCMs.

II.2 Trajectory model input

The trajectory model is driven by 6-hourly horizontal winds and 6-hourly average diabatic heating rates; water vapor is controlled by 6-hourly instantaneous temperatures. These fields come from the European Centre for Medium-Range Weather Forecasts (ECMWF) ERA-Interim (ERAi) data set, Goddard Earth Observing System Chemistry Climate Model (GEOSCCM), and the Whole Atmosphere Community Climate Model (WACCM).

ERAi is a global atmospheric reanalysis extending from 1979 onwards [Dee et al.,

2011]. For ERAi data, there are 60 hybrid levels extending from the surface to 0.1 hPa, with horizontal resolution of 1° latitude by 1° longitude. The GEOSCCM couples the GEOS-5 climate model to a comprehensive stratospheric chemistry module [Rienecker et al., 2008; Molod et al., 2012]. In this study, the simulation we use is from 1998 to 2099 and is driven by the Representative Concentration Pathway (RCP) 6.0 greenhouse gas scenario [Van Vuuren et al., 2011] and the A1 scenario for ozone depleting substances [World Meteorological Organization, 2011]. The model has horizontal resolution of 2° latitude by 2.5° longitude and 72 vertical levels up to the model top at 0.01 hPa. WACCM is a component of the National Center for Atmospheric Research (NCAR) Community Earth System Model (CESM), and the simulation we use is a specified chemistry version of WACCM (SC-WACCM), which is a model with prescribed trace gas concentrations and short wave heating rates from previous WACCM simulations. The simulation used here extends from 1955 to 2100 and is driven by the RCP 8.5 greenhouse gas scenario [Van Vuuren et al., 2011]. WACCM has 66 vertical layers from the surface to 5.1×10^{-6} hPa ($\sim$140 km) and its horizontal resolution is 1.9° latitude by 2.5° longitude [Marsh et al., 2013].

In this paper, we will first examine the tropical lower stratospheric water vapor from the GEOSCCM and WACCM. Then we will analyze output from the trajectory model driven by the ERAi (hereafter traj-ERAi), GEOSCCM (traj-GEOSCCM), and WACCM (traj-WACCM) in order to determine how well the CCMs reproduce the key processes that regulate the water vapor in tropical lower stratosphere.

II.3 Trajectory analyses of the mass of water vapor entering the stratosphere

In the trajectory analyses, we pay particular attention to the 380-K isentropic surface, which is close to the tropical tropopause and divides the stratosphere into the ”overworld” and the ”middleworld” [Hoskins, 1991]. We will use this level as the dividing line between the troposphere and stratosphere. If a parcel makes it to the 380-K level between $\pm$ 40° latitudes, we define that parcel to have entered the stratosphere. We are only concerned with the first time trajectories cross the 380-K surface between $\pm$ 40° latitudes, so additional crossings are not counted. On average, it takes 39 days for parcels to enter the stratosphere after initialization for all trajectory model runs.

We assume each parcel carries equal amount of air mass, so the mass of air carried by a group of parcels is proportional to the number of parcels in this group. When a parcel crosses the 380-K level, its water vapor mixing ratio is specifically identified ($[H_2O]_{380K}$). We define the mass of water vapor entering the stratosphere in a specific month, $m_{H_2O}^{entry}$, to be proportional to the sum of the $[H_2O]_{380K}$ in these parcels while they cross the 380-K surface during this month.

Finally, it should be noted that some dehydration can occur above the 380-K level. So the assumption that the mass of water vapor entering the stratosphere is equal to the flux through the 380-K surface will overestimate the moisture flux into the lower stratosphere. In Table 2.1 we show the percentage of FDPs that occur above the 380-K potential temperature surface in the traj-ERAi run, traj-GEOSCCM run, and traj-WACCM run respectively. We also show the average overestimation of the moisture flux into the lower

Table 2.1: FDP statistics in the trajectory model.

	traj-ERAi	traj-GEOSCCM	traj-WACCM
FDPs above 380-K	7%	7%	33%
overestimation	0.12 ppmv 4.46%	0.11 ppmv 3.13%	0.52 ppmv 15.29%

stratosphere, which is obtained by differencing $\overline{[H_2O]_{380K}}$ and $\overline{[H_2O]_{FDP}}$ (the average water vapor mixing ratio at the parcels' final dehydration point). This assumption results in a overestimation less than 10% in both the traj-ERAi run and traj-GEOSCCM run, with a slightly higher value for traj-WACCM. We only use this assumption that the mass of water vapor entering the stratosphere is equal to the flux through the 380-K surface in the section where we investigate the details of the transport of water vapor into the stratosphere. This assumption is not used in the analysis of the seasonal cycle of the tropical lower stratospheric water vapor, so the overestimation we discussed above is not included in the seasonal cycles we show.

III RESULTS

III.1 Tropical lower stratospheric water vapor in the GEOSCCM and WACCM

In this section, we investigate how well the GEOSCCM and WACCM reproduce the tropical lower stratospheric water vapor seasonal cycle during the period 2005 to 2014. In Fig. 3.1 we compare the seasonal cycle of the tropical lower stratospheric water vapor from the CCMs to that from the observation and the reanalysis. The observation of the seasonal cycle comes from the Earth Observing System (EOS) Microwave Limb Sounder (MLS) version 4.2 level 2 water vapor. We show the seasonal cycle of the 100-hPa water vapor mixing ratio (ppmv) averaged between 20°S - 20°N latitudes.

The GEOSCCM produces a seasonal cycle that generally agrees with the observation and reanalysis (panel (a)). The mean of the seasonal cycle simulated by the GEOSCCM (circular marker) is 0.28 ppmv lower than the MLS (dashed line) and 0.72 ppmv lower than the ERAi (solid line). The phase of the seasonal cycle in the GEOSCCM agrees with that from the MLS and ERAi. The peak-to-peak amplitude is close to the observation and the reanalysis, which is 0.38 ppmv smaller than that from the MLS and 0.05 ppmv smaller than that from the ERAi (panel (b)).

The WACCM, on the other hand, overestimates the average value of water vapor at 100 hPa and produces a weaker seasonal oscillation. The mean of the seasonal cycle from the WACCM (triangular marker, panel (a)) is 0.96 ppmv larger than that from the MLS and 0.52 ppmv larger than that from the ERAi. Since the WACCM produces a seasonal

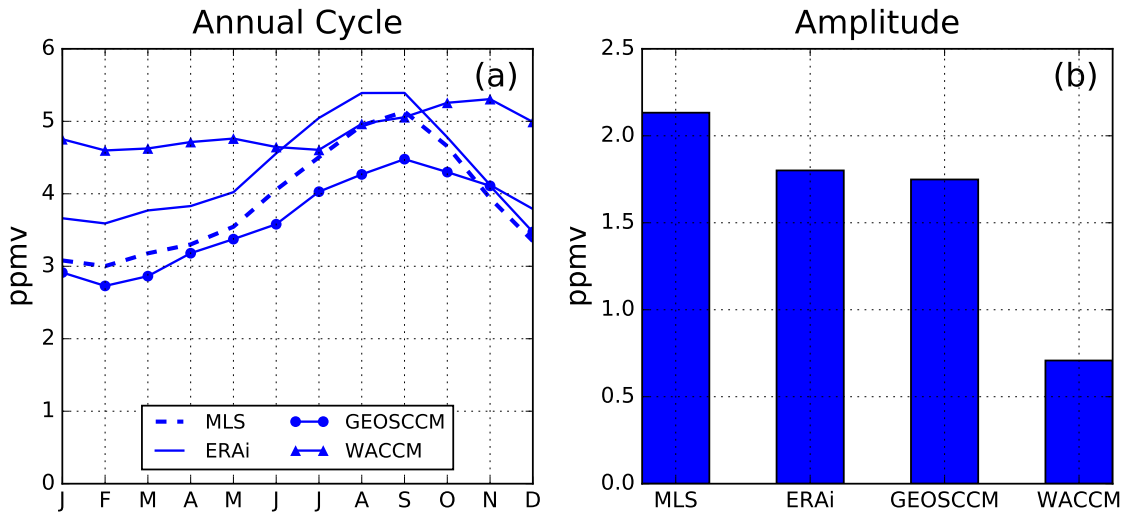

Figure 3.1: Seasonal cycle of 100-hPa water vapor (ppmv) averaged over the period from 2005 to 2014, between 20°S - 20°N latitudes. (a) The seasonal cycle. (b) The peak-to-peak amplitude.

cycle with maximum value similar to the observation and reanalysis, the overestimation in the mean comes from the overestimation of winter water vapor concentrations. This also means that the seasonal cycle from the WACCM is weaker, with an amplitude 1.42 ppmv smaller than the MLS and 1.09 ppmv smaller than the ERAi.

Fig. 3.2 provides a more comprehensive view of how well the GEOSCCM and WACCM reproduce the tropical lower stratospheric water vapor. We compare the water vapor distribution (ppmv) at 100 hPa from the two CCMs to that from the reanalysis and observation. Compared to the MLS (panels (a), (b), and (c)) and ERAi (panels (d), (e), and (f)), the GEOSCCM generally does a good job reproducing the annual average (panel (g)) and the boreal winter (panel (i)) water vapor distribution. During boreal summer (panel (h)), however, the GEOSCCM overestimates the water vapor concentration in the Sub-tropical West Pacific and underestimates water vapor concentration in the deep tropics and

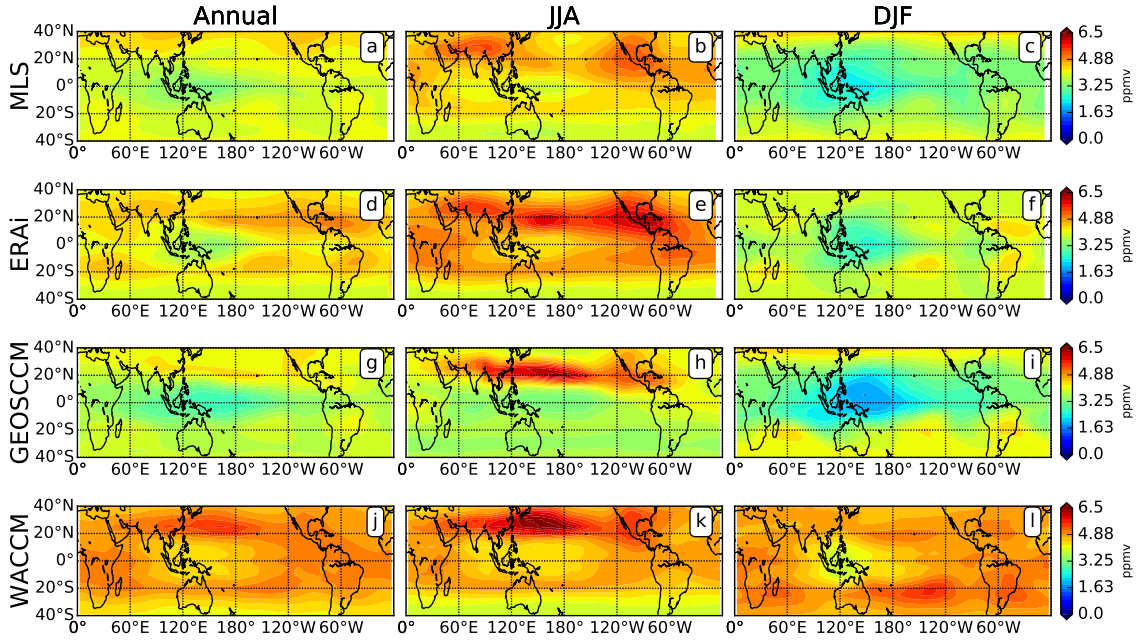

Figure 3.2: Water vapor mixing ratio (ppmv) at 100 hPa between 40°N and 40°S during the period 2005 to 2014. First row (a-c): MLS; Second row (d-f): ERAi; Third row (g-i): GEOSCCM; Fourth row (j-l): WACCM. First column (a, d, g, and j): annual average; Second column (b, e, h, and k): boreal summer (JJA); Third column (c, f, i, and l): boreal winter (DJF).

the southern hemisphere. The WACCM overall produces higher water vapor concentration (panels (j), (k), and (l)). In particular, the boreal winter water vapor concentration in the WACCM is on average 1.29 ppmv and 1.02 ppmv larger than that in the MLS and in the ERAi respectively. The overestimation of the water vapor in boreal winter results in a weaker seasonal contrast in the WACCM, which is also shown in the seasonal cycle (Fig. 3.1).

In order to investigate the drivers of the seasonal cycle, we calculate the transport of water vapor across the 100-hPa surface, which is quantified by the water vapor mass flux. To do this, we multiply the water vapor amount by the potential temperature tendency ($\frac{d\theta}{dt}$,

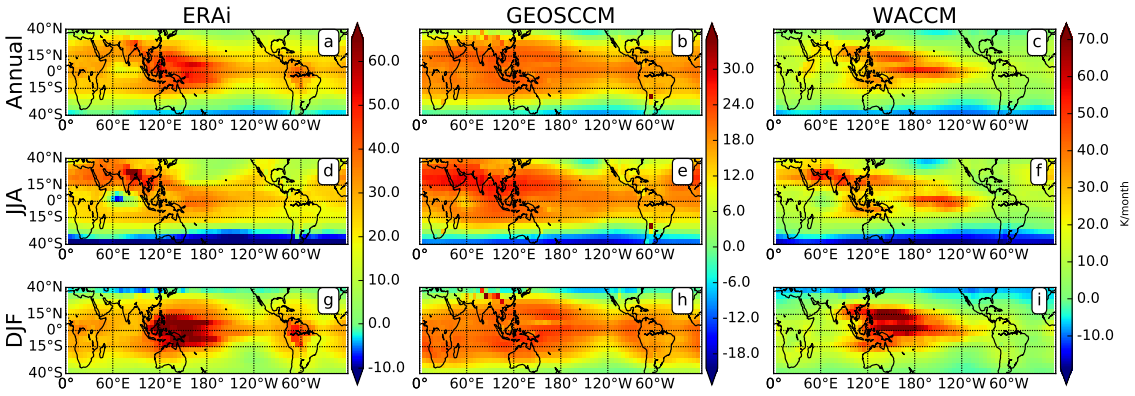

Figure 3.3: Potential temperature tendency ($K/month$) at 100 hPa between 40°N and 40°S during the period 2005 to 2014. First row (a-c): annual average; Second row (d-f): boreal summer (JJA); Third row (g-i): boreal winter (DJF). First column (a, d, and g): ERAi; Second column (b, e, and h): GEOSCCM; Third column (c, f, and i): WACCM.

Fig. 3.3) deduced from the diabatic heating rates. Fig. 3.4 shows the water vapor mass flux in the ERAi and the CCMs.

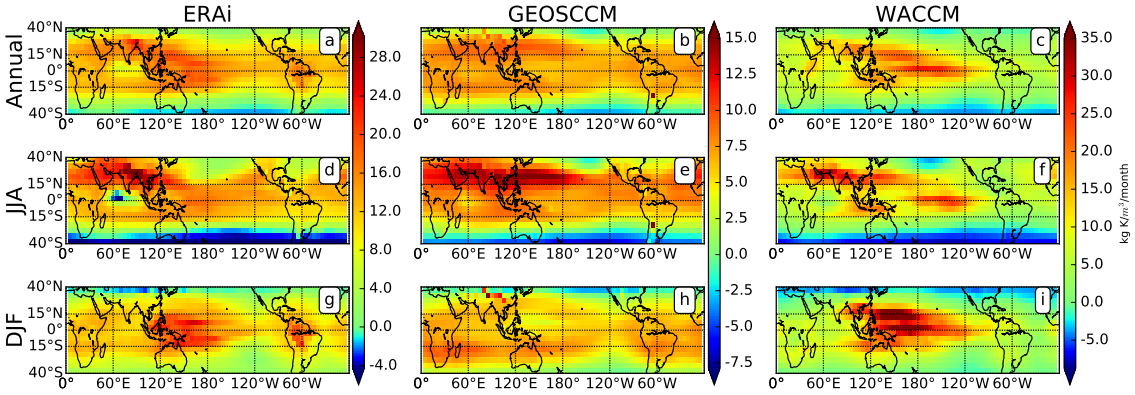

Figure 3.4: The water vapor mass flux ($kg \cdot K/m^2/month$) at 100 hPa between 40°N and 40°S during the period 2005 to 2014. First row (a-c): annual average; Second row (d-f): boreal summer (JJA); Third row (g-i): boreal winter (DJF). First column (a, d, and g): ERAi; Second column (b, e, and h): GEOSCCM; Third column (c, f, and i): WACCM.

The annual average distribution from the ERAi (Fig. 3.4a) shows that the upward transport of water vapor into the stratosphere locates in the deep tropics between 15°N and 15°S. In the deep tropics, the flux is particularly strong in the Tropical West Pacific.

Other important regions include South Asia, Tropical Africa and South America. These are also regions of strong upward motion through the 100-hPa surface (Fig. 3.3a). In boreal summer (Fig. 3.4d), stronger water vapor mass flux lies in the Asian monsoon region, the Tropical West Pacific, and the Central to East Pacific. In boreal winter (panel (g)), the water vapor mass flux is strong in the Tropical West Pacific and South America. Note the distribution of the ERAi flux closely mirrors the distribution of the ERAi potential temperature tendency (panels (a), (d), and (g), Fig. 3.3) in the annual average and in boreal summer and winter. This suggests that the water vapor mass flux into the stratosphere is mainly controlled by the upward motion through the tropopause and that the spatial variability in the water vapor concentration plays a smaller role.

The distribution of water vapor mass flux in the GEOSCCM (panels (b), (e), and (h), Fig. 3.4) shows a similar pattern compared to that in the ERAi. However, the magnitude of the flux in the GEOSCCM is much smaller, which is attributed to the weaker upward motion at 100 hPa in the GEOSCCM (panels (b), (e), and (h), Fig. 3.3). This is particularly apparent in the Tropical West Pacific. In boreal summer (panel (e)), the GEOSCCM overestimates the dominance of upward transport of water vapor in the Subtropical West Pacific and underestimates the dominance in the Tropical West Pacific, which is consistent with the distribution of 100-hPa water vapor concentration in the GEOSCCM (Fig. 3.2h).

The WACCM (panels (c), (f), and (i), Fig. 3.4) shows reasonable agreement in the Tropical West Pacific in the annual average and in boreal summer and winter. In boreal summer, the water vapor mass flux in the Asian monsoon region and East Pacific is largely

underestimated (panel (f)). In boreal winter, the water vapor mass flux is underestimated in Africa and South America (panel (i)). The potential tendency at 100 hPa in the WACCM (panels (c), (f), and (i), Fig. 3.3) shows a localized pattern confined in the Tropical West Pacific region, which explains the dominance of the upward water vapor mass flux in that region.

In summary, there's general agreement between the tropical lower stratospheric water vapor in the MLS, the ERAi, and the GEOSCCM in terms of the seasonal cycle, the horizontal distribution of water vapor, and the distribution of water vapor mass flux across the 100-hPa surface. The WACCM, however, shows weaker seasonal variability in the 100-hPa water vapor and shows localized water vapor mass flux in the Tropical West Pacific region. The key dynamical processes that regulate the tropical lower stratospheric water vapor in both CCMs still need to be investigated in detail.

III.2 Investigation of the key processes using the trajectory model

Before diving into the details of the key processes, we first validate the seasonal cycle of the tropical lower stratospheric water vapor simulated by the trajectory model compared to that from the observation and the two CCMs to show any bias that may exist in the trajectory model. Since the diabatic trajectory model uses an isentropic vertical coordinate, in the trajectory analyses we are going to show results on isentropic levels instead of isobaric levels. The seasonal cycle is defined to be the monthly water vapor mixing ratio (ppmv) averaged over the period 2005 to 2014, between 20°S - 20°N latitudes and 380 K - 390 K potential temperatures.

Fig. 3.5 shows that the seasonal cycle simulated by the traj-ERAi run (solid orange line, panel (a)) is on average 1.03 ppmv lower than that from the MLS (solid blue line, panel (a)). In our trajectory runs, we didn't include adjustments for cloud physics [Jensen et al., 2001] or the moistening effect of anvil ice from convective overshooting [e.g. Dessler, 2002; Jensen et al., 2007; Dessler et al., 2007], which results in an underestimation of the water vapor in the trajectory model compared to the MLS [Schoeberl et al., 2014]. However, the trajectory model does a good job reproducing the seasonal variability: the phase and the amplitude of the seasonal cycle from the traj-ERAi run is almost the same with that from the MLS. This suggests that the trajectory model well reproduces the seasonal oscillation of the tropical lower stratospheric water vapor in spite of the missing processes. We also infer that the seasonal oscillation of the tropical lower stratospheric water vapor is primarily driven by the TTL temperatures, which confirms Mote et al., [1996].

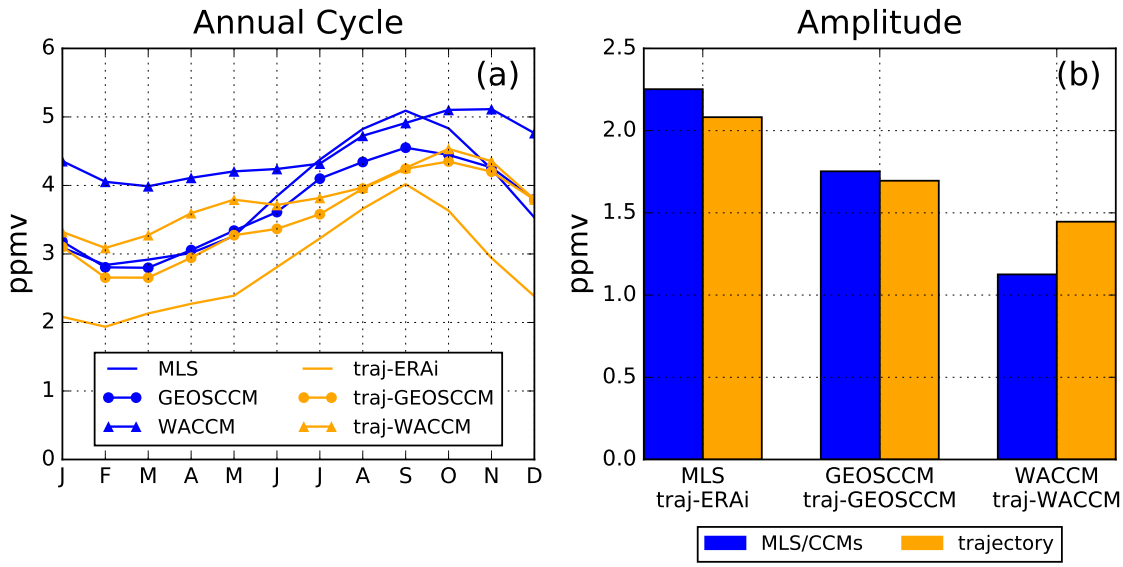

Figure 3.5: The season cycle of water vapor (ppmv) averaged over the period 2005 to 2014, between 20°S - 20°N latitudes and 380 K - 390 K potential temperatures. The seasonal cycle is from the MLS, GEOSCCM, WACCM, and the trajectory model driven by the ERAi and CCMs. (a) The seasonal cycle. (b) The peak-to-peak amplitude.

The seasonal cycle simulated by the traj-GEOSCCM run (orange line with circular marker, Fig. 3.5a) has a mean 0.18 ppmv smaller than that from the GEOSCCM (blue line with circular marker, Fig. 3.5a). But the amplitude of the seasonal cycle from the traj-GEOSCCM run is similar to that from the GEOSCCM (Fig. 3.5b). The seasonal cycle simulated by the traj-WACCM run (orange line with triangular marker, Fig. 3.5a) is on average 0.69 ppmv lower than that from the WACCM (blue line with triangular marker, Fig. 3.5a), with 0.97 ppmv underestimation in February in particular. The underestimation of the minimum by the trajectory model also leads to an overestimation of the amplitude (Fig. 3.5b), and specifically the amplitude is 0.32 ppmv larger than that from the WACCM. Note both the traj-WACCM run and WACCM produce weaker seasonal cycles than the observation, which suggests that the weaker seasonality is attributed to weaker seasonal

oscillation in the TTL temperatures in the WACCM.

In summary, there is general agreement between the seasonal cycles from the MLS, the CCMs, and the trajectory models driven by reanalysis and CCM winds. Controlled by large-scale transport and TTL temperature, the trajectory model does a good job reproducing the seasonal variability of the tropical lower stratospheric water vapor in the observation and the CCMs. Therefore the trajectory model can be an appropriate tool to evaluate the large-scale mechanisms regulating the seasonal cycle of the tropical lower stratospheric water vapor in the CCMs.

III.2.1 The transport of water vapor into the stratosphere

We now examine the details of the transport of water vapor into the stratosphere in the trajectory models. First, we trace parcels entering the stratosphere back to 360 K to determine where stratosphere-bound parcels are crossing the 360-K surface, thereby quantifying TTL transport within the models. Specifically, we examine the contribution to $m_{H_2O}^{entry}$ from the 360-K level. To calculate this quantity, we collect all parcels crossing the 380-K surface during each month and bin parcels by the latitude and longitude of the parcels' location when at 360 K. Then we sum the $[H_2O]_{380K}$ (as defined in Section 2.3) in each bin and divide that by the total $[H_2O]_{380K}$ in all of the bins.

Fig. 3.6 shows the contribution to $m_{H_2O}^{entry}$ from the 360-K level in our trajectory model. In the traj-ERAi run, we see that mass of water vapor in the lower stratosphere generally originates between 15°N and 15°S on an annual average basis (panel (a)). In boreal summer (JJA), more water vapor originates from Asian monsoon region, Subtropical West Pacific,

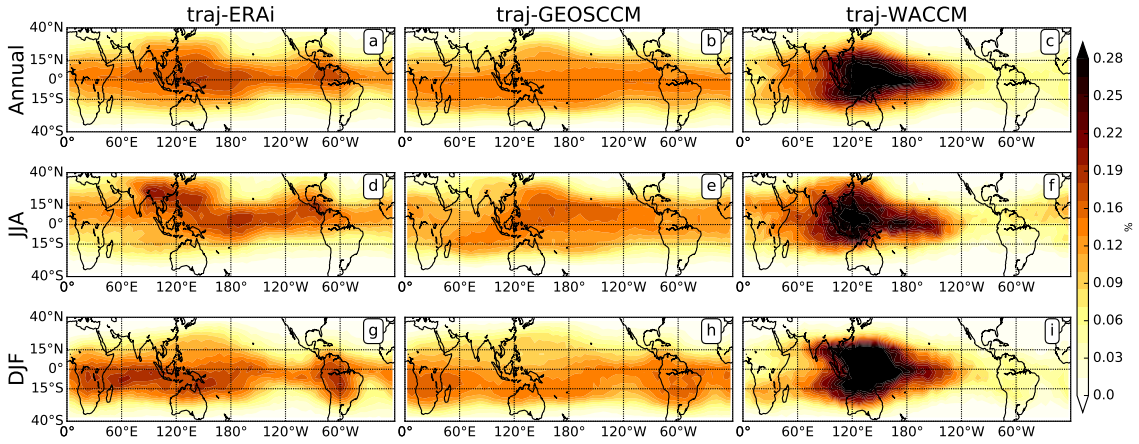

Figure 3.6: Contribution (%) to $m_{H_2O}^{entry}$ from 360-K level during the period from 2005 to 2014. First row (a-c): annual average; Second row (d-f): boreal summer (JJA); Third row (g-i): boreal winter (DJF). First column (a, d, and g): traj-ERAi run; Second column (b, e, and h): traj-GEOSCCM run; Third column (c, f, and i): traj-WACCM run.

Tropical West Pacific, and East Pacific (panel (d)). In boreal winter (DJF), more water vapor originates from Tropical Africa, the monsoon region near Australia, and Tropical America (panel (g)).

We have shown the water vapor mass flux at 100 hPa in the ERAi and CCMs (Fig. 3.4), which allows us to examine where most water vapor enters the stratosphere. The differences between Figures 3.6 and 3.4 show that moisture is horizontally transported while it travels upward into the stratosphere, so it reaches the 100-hPa surface at different locations from its initialization point. This agrees with previous studies that pointed out the importance of horizontal movement during the troposphere-to-stratosphere transport (TST) of air parcels [e.g. Holton and Gettelman, 2001; Fueglistaler et al., 2004; Bonazzola and Haynes, 2004; Levine et al., 2007]. This is particularly apparent in boreal summer: even though the Subtropical West Pacific is one of the major source regions at the 360-K

initialization level for stratospheric moisture (Fig. 3.6d), it is not as dominant a region for water vapor to enter the stratosphere (Fig. 3.4d).

The features discussed above are generally well reproduced by the traj-GEOSCCM run (panels (b), (e), and (h)). But the traj-GEOSCCM run shows general underestimation in the contributions compared to the result from the traj-ERAi run, especially in the Asian monsoon region in boreal summer (panel (e)). The result from the traj-WACCM run shows larger differences, including more intense regional contributions compared to the traj-ERAi and traj-GEOSCCM run (panels (c), (f), and (i)). Specifically, the traj-WACCM run substantially overestimates the contribution from the Tropical West Pacific region throughout the year, while it underestimates the JJA contribution from the East Pacific and the DJF contribution from Tropical Africa and Tropical America.

III.2.2 Location of final dehydration

As explained in Section 2.1, a parcel dehydrates if its RH exceeds the predetermined saturation threshold, and this may occur multiple times along its trajectory. Therefore, the final dehydration point (FDP) of parcels plays a crucial role in determining the concentration of stratospheric water vapor. In this section, we test how well the CCMs reproduce the location of FDPs.

Fig. 3.7 shows the horizontal distribution of FDPs. The horizontal distribution is obtained by counting the number of parcels that reach their FDP in each equal area latitude-longitude grid box ($\sim 5°$ by $5°$) at all altitudes and then dividing it by the total number of parcels that reach FDP at all locations.

The traj-ERAi run shows that the FDP maxima are located in the deep tropics between 15°S and 15°N, and that few FDPs occur in the subtropics. Specifically, the annual average result from the traj-ERAi run (panel (a)) shows that the dominant region for FDP is the Tropical West Pacific, where the TST of water vapor is strong (Figures 3.4 and 3.6) and the temperatures tend to be low [Fueglistaler et al., 2009]. The distribution there shows a symmetric pattern, with maxima located both north and south of the equator. Other FDP maxima include Tropical Africa, South Asia, and South America. In boreal summer (Fig. 3.7d), FDPs are located in South Asia and the tropical Pacific. Few JJA FDPs occur in the northern hemisphere subtropics, which suggests that although this latitude range is important for the TST of water vapor in summer (Figures 3.4 and 3.6), it plays a minor role in the dehydration of the stratospheric water vapor. Finally the DJF FDPs (Fig. 3.7g) are found in the Tropical West Pacific, South America, and Tropical Africa.

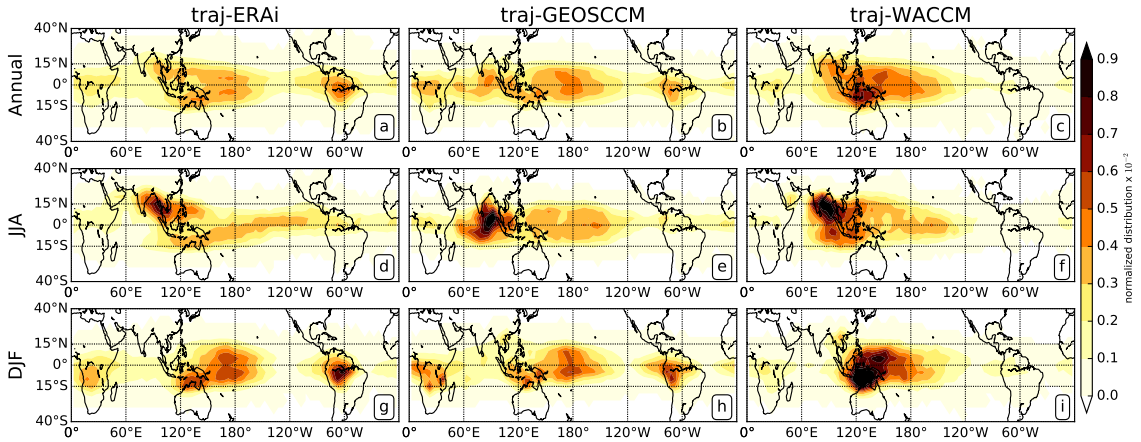

Figure 3.7: Horizontal distribution of FDPs (normalized distribution $\times 10^{-2}$) for all parcels that enter the stratosphere between 40° N and 40° S, during the period from 2005 to 2014. First row (a-c): annual average; Second row (d-f): boreal summer (JJA); Third row (g-i): boreal winter (DJF). First column (a, d, and g): traj-ERAi run; Second column (b, e, and h): traj-GEOSCCM run; Third column (c, f, and i): traj-WACCM run.

The traj-GEOSCCM run does a good job reproducing the annual average and winter FDPs in the traj-ERAi run. But in summer (Fig. 3.7e), the traj-GEOSCCM run shows higher FDP density in the Indian Ocean and lower FDP density in South Asia compared to the traj-ERAi run. The summer upward motion distribution from the ERAi shows a local minimum in the Indian Ocean (Fig. 3.3d), but the GEOSCCM failed to reproduce this feature and underestimates the upward motion in South Asia (Fig. 3.3e). These are consistent with the differences in the FDP pattern between the traj-GEOSCCM run and the traj-ERAi run.

The horizontal distributions of FDPs in the traj-WACCM run shows larger differences. Both the annual average (Fig. 3.7d) and the DJF (Fig. 3.7i) FDP density show substantial overestimation in the Tropical West Pacific and underestimation in Tropical Africa and South America. In the Tropical West Pacific, the traj-WACCM run shows too high of a density just south of the equator. During summer, the FDP density in the traj-WACCM run shows an overestimation in South Asia (panel (c)). These overestimation and underestimation in the traj-WACCM run are consistent with the differences in the TTL transport pattern compared to that in the traj-ERAi run (Figures 3.4 and 3.6).

The annual average vertical distribution of FDPs is shown in Fig. 3.8, with annual temperature fields over-plotted. The vertical distribution is obtained in the same method as the horizontal distribution using latitude-potential temperature grid boxes ($\sim 5°$ by 2 K). In the traj-ERAi run (panel (a)), most FDPs occur at the 368-K isentropic surface among the coldest levels in the TTL, and only about 7% of the parcels have FDPs above the 380-

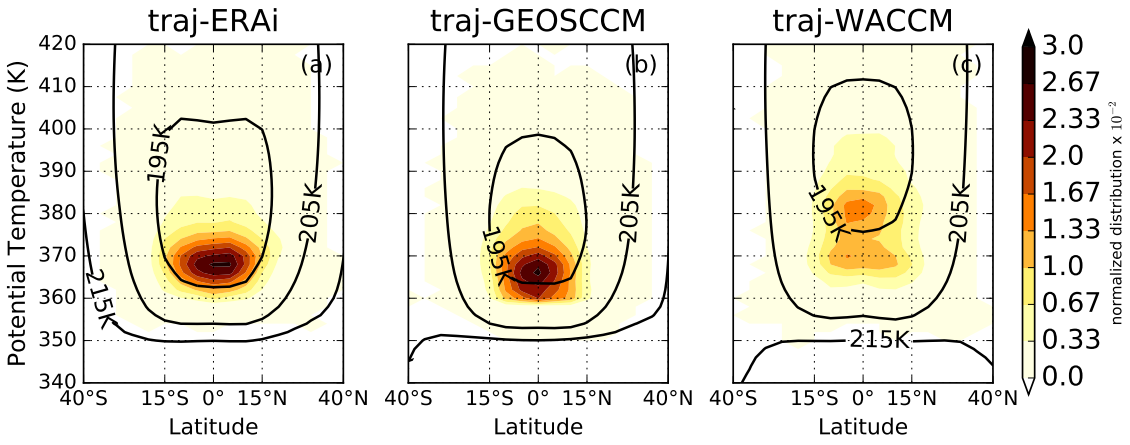

Figure 3.8: Annual average vertical distribution of FDPs (normalized distribution $\times 10^{-2}$) for all parcels that enter the stratosphere between 40°N and 40°S during 2005-2014, with annual average zonal mean temperature contours over-plotted.

K surface (Table 2.1). So the amount of moisture entering the stratosphere is basically determined before parcels cross the 380-K surface.

The vertical distribution of FDPs produced by the traj-GEOSCCM run captures the features of the traj-ERAi run well (panel (b)). Most FDPs in the traj-GEOSCCM run occur at 366-K isentropic surface, and only 7% of the parcels dehydrate above the 380-K surface. The vertical distribution of FDPs produced by the traj-WACCM run, on the other hand, shows more significant differences (panel (c)). First the temperature field shows the cold region in the WACCM is centered at higher levels than that in the ERAi. This results in FDPs being higher in the traj-WACCM run, with 33% of the parcels dehydrating above the 380-K surface. In addition, the traj-WACCM run shows, in the deep tropics, there's a higher FDP density in the Southern Hemisphere, which is the same overestimation in southern Tropical West Pacific seen in the horizontal distribution in Fig. 3.7.

III.2.3 The regional contribution to the seasonal cycle

In previous sections we showed that the deep tropics between 15°S and 15°N dominates both the annual transport of water vapor into the stratosphere and the annual final dehydration, while the northern hemisphere subtropics (15°N - 40°N) plays an important role in the summer TST of water vapor. The CCMs do a good job reproducing these features. In this section, we focus our investigation on how well the CCMs reproduce the contribution to the seasonal cycle of the tropical lower stratospheric water vapor from the three latitude bands: 40°S - 15°S (SH), 15°S - 15°N (TR), and 15°N - 40°N (NH). The seasonal cycle is the monthly water vapor mixing ratio (ppmv) averaged over the period 2005 to 2014, between 20°S - 20°N latitudes and 380 K - 390 K potential temperatures.

We investigate the contribution from the three latitude bands at two isentropic levels respectively, including the 360-K level and the 380-K level. For the 360-K level, we examine $cycle(SH_{360K})$, $cycle(TR_{360K})$, and $cycle(NH_{360K})$. These are seasonal cycles in the trajectory model including just the water vapor from parcels initialized in SH, TR, and NH respectively. This is achieved by first identifying all the parcels initialized in a specific latitude band and then removing water vapor from all parcels outside that latitude range. For the 380-K level, we examine $cycle(SH_{380K})$, $cycle(TR_{380K})$, and $cycle(NH_{380K})$, which are seasonal cycles computed using the same method, including just the water vapor from parcels that go through SH, TR, and NH at the 380-K surface.

We first compare these seasonal cycles with the reference seasonal cycle (the seasonal cycle without removal of any water vapor) in Fig. 3.9. Based on the $cycle(SH_{360K})$,

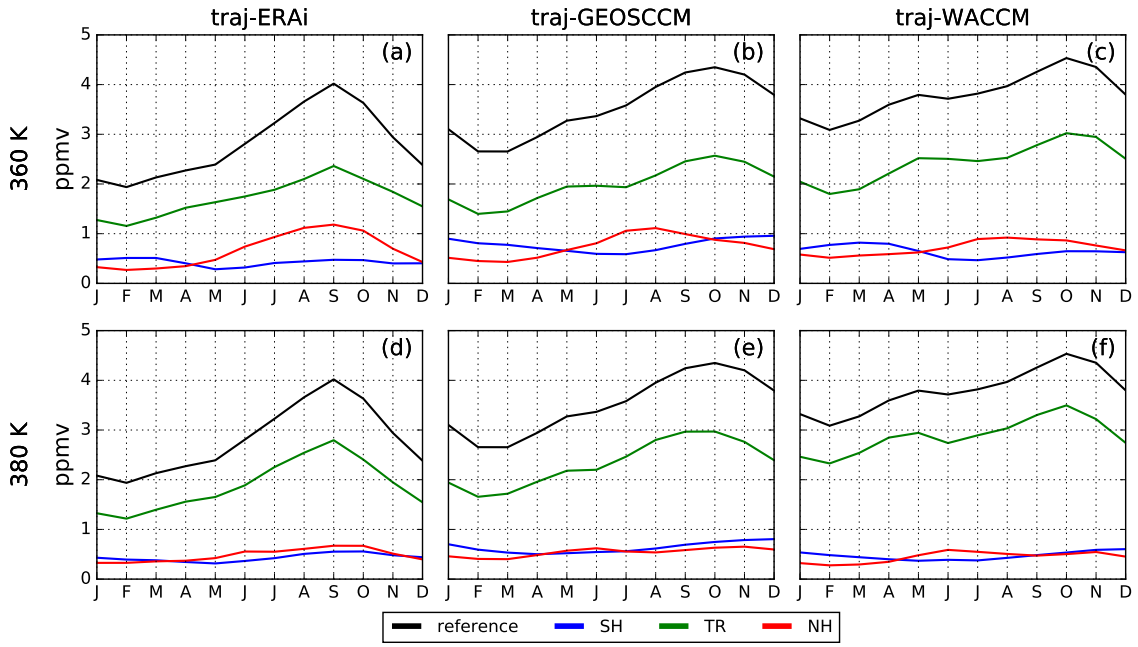

Figure 3.9: Comparison between the reference seasonal cycle (black) simulated by the trajectory model and the $cycle(SH_{360K})$ (blue), $cycle(TR_{360K})$ (green), and $cycle(NH_{360K})$ (red) (a - c), and the $cycle(SH_{380K})$ (blue), $cycle(TR_{380K})$ (green), and $cycle(NH_{380K})$ (red) (d - f). First column (a and d): traj-ERAi run; Second column (b and e): traj-GEOSCCM run; Third column (c and f): traj-WACCM run.

$cycle(TR_{360K})$, and $cycle(NH_{360K})$ in the traj-ERAi run (panel (a)), we see that the seasonal cycle is dominated by the $cycle(TR_{360K})$ (green), which is perfectly in phase with the reference seasonal cycle and has larger water vapor value than $cycle(NH_{360K})$ (red) and $cycle(SH_{360K})$ (blue). The $cycle(NH_{360K})$ is also in phase with the reference seasonal cycle, but the seasonal oscillation is weaker. The $cycle(SH_{360K})$, however, shows little seasonal variability. Similar to Fig. 3.9a, Fig. 3.9d shows that the seasonal cycle is dominated by $cycle(TR_{380K})$.

The result from the traj-GEOSCCM run (Figures 3.9b and 3.9e) and the traj-WACCM run (Figures 3.9c and 3.9f) agree with the traj-ERAi run that the seasonal cycle is dominated

by the parcels initialized and entering the stratosphere in the TR. But the $cycle(NH_{360K})$, $cycle(SH_{360K})$, $cycle(NH_{380K})$, and $cycle(SH_{380K})$ show differences compared to the traj-ERAi run. Specifically, the $cycle(NH_{360K})$ in the trajectory driven by the CCMs are not in phase with the reference seasonal cycle, peaking two or three months earlier than the reference seasonal cycle. Meanwhile the $cycle(SH_{360K})$ in the trajectory driven by the CCMs has an almost opposite phase compared to the reference seasonal cycle (panels (b) and (c)). The $cycle(NH_{380K})$ and $cycle(SH_{380K})$ show similar features as the $cycle(NH_{360K})$ and $cycle(SH_{360K})$, but with weaker seasonal oscillation.

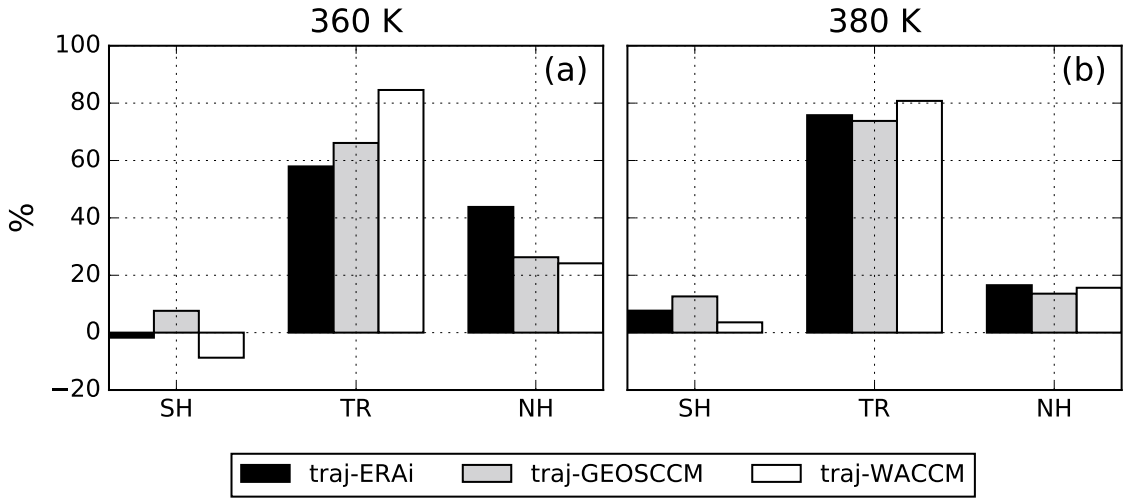

Figure 3.10: Contribution (%) from the SH, TR, and NH (a) at 360-K level and (b) at 380-K to seasonal oscillation.

We also examine the contribution from the latitude bands to the seasonal oscillation of the tropical lower stratospheric water vapor quantitatively. To do this, we first compute the peak-to-peak amplitude of the reference seasonal cycle, and record the month when the reference seasonal cycle reaches minimum (t_{min}) and the month when the reference seasonal cycle reaches maximum (t_{max}). Then for each $cycle(SH_{360K})$, $cycle(TR_{360K})$,

$cycle(NH_{360K})$, $cycle(SH_{380K})$, $cycle(TR_{380K})$, and $cycle(NH_{380K})$ we compute the difference between the water vapor mixing ratios during t_{max} and t_{min} and divide it by the peak-to-peak amplitude of the reference seasonal cycle.

The contributions to the seasonal oscillation in the traj-ERAi run (black bars in Fig. 3.10) show that, at both the 360-K level and 380-K level, the TR is the dominant contributor, with contributions of 58% (Fig. 3.10a) and 76% (Fig. 3.10b) respectively. This is consistent with our results in the previous sections. The TR dominates the transport of water vapor into the stratosphere (Figures 3.3 and 3.6) and is the most important latitude range for parcels' final dehydration (Fig. 3.7), therefore the seasonal variability of the tropical lower stratospheric water vapor is dominated by this latitude range.

Previous studies [e.g. Bonazzola and Haynes, 2004; Gettelman et al., 2004] and our result from the traj-ERAi run (Figures 3.4 and 3.6) show that the troposphere-to-stratosphere transport of water vapor in the Asian monsoon region has strong seasonal variability, and that it is particularly strong in summer. But Fig. 3.10 shows that, compared to the TR, the NH latitude band as a whole makes a smaller contribution to the seasonal oscillation of the tropical lower stratospheric water vapor. This suggests that the strong transport of water vapor into the stratosphere during summer in the Asian monsoon region alone isn't the major contributor to the seasonal oscillation of the tropical lower stratospheric water vapor. This agrees with the result from Wright et al. [2011], who used a similar method to explore the contribution from the South Asian summer convection to the mean water vapor at 68 hPa.

The contributions to the seasonal oscillation in the traj-GEOSCCM run and the traj-WACCM run are generally similar to those in the traj-ERAi run. Some differences exist in the contributions from the 360-K level. The contribution from the TR is overestimated and the contribution from the NH is underestimated in the traj-GEOSCCM run (gray bars, panel (a)). This is consistent with the underestimation in the contribution to $m_{H_2O}^{entry}$ from the 360-K level in the Asian monsoon region (Fig. 3.6d). Further more, the SH contributes negatively to the seasonal oscillation in the traj-ERAi run, but the traj-GEOSCCM run failed to reproduce this feature. The traj-WACCM run also overestimates the contribution from the TR and underestimates the contribution from the NH at the 360-K level (white bar, panel (a)). Finally, the contributions from the three latitude bands at the 380-K level produced by the two traj-CCM runs are consistent with those in the traj-ERAi run (panel (b)).

III.3 The CCM predictions in a changing climate

In previous sections we showed that the CCMs generally do well in reproducing the seasonal cycle of the tropical lower stratospheric water vapor and the key processes that regulate it, which indicates the CCMs may provide insight in the stratospheric water vapor in a changing climate. In this section we investigate how the seasonal cycle of the tropical lower stratospheric water vapor changes and how the FDPs change during the 21st century in the CCMs and in the trajectory model driven by the CCMs.

III.3.1 The seasonal cycle during 2089-2098

Both CCMs predict that the seasonal cycle will be moister in all months by the end of the century (blue lines, Figures 3.11a and 3.11b), with a larger increase of moisture in the WACCM in all months than in the GEOSCCM (blue lines with plus marker, Figures 3.11c and 3.11d). Meanwhile, the amplitude of the seasonal cycle also changes. The GEOSCCM shows a stronger seasonal cycle (blue dashed line, Figures 3.11a), with 0.64 ppmv (36%) increase in the amplitude (Table 3.1). The WACCM, however, shows a weaker seasonal cycle (blue dashed line, Figures 3.11b), with 0.32 ppmv (28%) decrease in the amplitude (Table 3.1). Finally, both the GEOSCCM and the WACCM predict the phase of the seasonally cycle will remain about the same.

We also examine how the trajectory model driven by the two CCMs reproduce the features discussed above (orange, Figures 3.11a and 3.11b). First, both the trajectory model runs agree with the CCMs that the phase of the seasonal cycle is predicted to show little change in both trajectory runs. Second, the trajectory runs also predict the moisture in

the seasonal cycle will increase by the end of the 21st century. However, the increase in the moisture of the seasonal cycle predicted by the traj-GEOSCCM run is not as large as that predicted by the GEOSCCM. There's around 0.5 ppmv of increase in the annual mean missing in the traj-GEOSCCM run (Table 3.1) and in September the traj-GEOSCCM underestimates the increase by 0.98 ppmv (Fig. 3.11c). Finally, the prediction of the amplitude of the seasonal cycle in the trajectory runs also differ from that in the CCMs. Both the trajectory runs predict that the amplitude of the seasonal cycle will remain almost the same during the century.

One possible issue in the trajectory models is their neglect of evaporation of convectively lofted ice. The evaporation of lofted ice has a moistening effect on the air in the lower stratosphere [e.g. Dessler, 2002; Jensen et al., 2007; Dessler et al., 2007; Grosvenor et al., 2007; Schoeberl et al., 2014], and Dessler et al. [2016] pointed out that an important part of the changes of tropical lower stratosphere moisture over the 21st century in these two CCMs can be explained by the changes in the evaporation of lofted ice. We found that the trajectory model does a better job reproducing the changes in both the mean value and the amplitude of the season cycle during the century when convectively lofted ice data from the GEOSCCM and WACCM is added (not shown). So the neglect of this process is responsible for an important part of the differences between the trajectory model and the CCMs.

Table 3.1: Change in the mean and amplitude of the season cycle of the tropical lower stratospheric water vapor by the end of the 21st century.

	MEAN		AMPLITUDE	
	GEOSCCM	WACCM	GEOSCCM	WACCM
CCM	0.93 ppmv 25%	1.85 ppmv 41%	0.64 ppmv 36%	-0.32 ppmv -28%
traj-CCM	0.44 ppmv 12%	1.88 ppmv 49%	0.06 ppmv 3%	0.14 ppmv 9%

III.3.2 Location of final dehydration during 2089-2098

Previous studies suggested that the long-term changes in the stratospheric water vapor are largely attributable to the changes of temperatures at the coldest levels in the TTL [e.g. Fueglistaler and Haynes, 2005; Oman et al., 2008; Gettelman et al., 2009; Kim et al., 2013]. Changes in these temperatures may therefore lead to important changes in the final dehydration point (FDP) of parcels, and further result in changes in the tropical lower stratospheric water vapor. In this section, we show how the FDPs change during the 21st century in the trajectory runs. The change in the FDPs is obtained by differencing the FDP distribution during 2089 - 2098 and the FDP distribution during 2005 - 2014.

Fig. 3.12 shows how the annual average horizontal distribution of FDPs change during the 21st century in the trajectory runs, with the change of the average temperatures at the coldest levels (black) over plotted. The traj-GEOSCCM run predicts that the FDPs will increase in the Tropical West Pacific and Tropical Africa, and that the FDPs will decrease in the Indian Ocean, East Pacific, and the Atlantic (panel (a)). The change in the average temperatures at the coldest levels (360 K - 400 K potential temperatures) plays an important role in changing the FDP pattern horizontally. While temperatures increase everywhere in

the TTL, the increase of the FDPs occurs in the Tropical West Pacific where the increase in the temperatures is the smallest, and the decrease of the FDPs occurs in most of the other tropical regions where the increase of the temperatures is larger. Notice the increase of the average temperatures at the coldest levels show maxima in the Asian monsoon region, but since there's few FDPs in that region both during 2005 to 2014 and during 2089 to 2098, the traj-GEOSCCM run shows little change in the FDP density there.

The traj-WACCM run predicts that there will be more FDPs occurring in the Tropical Africa and the Central and East Pacific, and fewer FDPs in the Tropical West Pacific, Indian Ocean, and northern Australia (Fig. 3.12b). The change in the temperatures at the coldest levels (360 K - 420 K potential temperatures) from the WACCM shows a different pattern compared to that from the GEOSCCM, which leads to a different pattern of the changes in the FDP density. There's maximum increase of the temperatures in the Indian Ocean and the Tropical West Pacific, which results in the decrease of the FDPs in the Indian Ocean, the Indonesian region, and northern Australia. While more parcels will have FDPs in other regions where the temperatures show a less intense increase, including the Tropical Africa and the East Pacific.

Fig. 3.13 shows the latitude-potential temperature distribution of changes in the FDPs during the 21st century, with the change of the temperature field (black) and the 2005-2014 temperature field (gray) over plotted. In the traj-GEOSCCM run, the change in the TTL temperature also plays an important role in changing the FDP pattern vertically (panel (a)). Specifically, there will be a more intense increase in temperatures at the lower

bound of the coldest region, which leads to more FDPs occurring at higher levels in the deep tropics and fewer FDPs occurring at lower levels. Figures 3.12a and 3.13a together show that the FDPs will mainly increase in the Tropical West Pacific between 380-K and 390-K isentropic surfaces and decrease in most of the other tropical regions at the lower bound of the coldest region.

The latitude-potential temperature distribution in the traj-WACCM run predicts that the FDPs in almost all locations in the tropics between $\pm$ 15° latitudes will take a large step upward (Figure 3.13b). The temperature field during 2005-2014 and the change of temperatures in the WACCM show that the most intense increase of temperatures will occur around the center of the coldest region in the TTL, and that a decrease of temperatures will occur at the top of the TTL. Therefore, the coldest region in the TTL will be located at a higher altitude during 2089-2098 in the WACCM. As a result, the increase in the FDPs reaches a level as high as $\sim$ 420-K potential temperature, and the decrease of FDPs at the lower bound of the coldest region reaches a level as high as $\sim$ 388-K. Figures 3.12b and 3.13b together show that the FDPs will mainly decrease in the Tropical West Pacific, the Indian Ocean, and northern Australia below the coldest region, and increase in the Tropical Africa and the Central and East Pacific at levels above the 382-K isentropic surface.

Finally, we focus on the annual cycle of the altitude of FDPs. We examine the weighted-average FDP level, which is the average isentropic level when weighted by the number of FDPs at each level. Figure 3.14a shows the monthly weighted-average FDP level simulated by the traj-ERAi run and the trajectory model driven by the CCMs during

2005 to 2014, as well as the monthly weighted-average FDP level predicted by the trajectory model driven by the CCMs during 2089 to 2098. During 2005 to 2014, the traj-ERAi run (solid line) finds an average FDP level between 370-K and 375-K potential temperatures throughout the year. There's some seasonality in the FDP level, with the summer level being lower than winter. In summer, parcels dehydrate at lower levels, where the temperatures are higher, bringing moister air into the stratosphere, but this plays a minor role regulating the seasonal cycle of the tropical lower stratospheric water vapor compared to the seasonal oscillation of the TTL temperatures.

During 2005 to 2014, the annual cycle of FDP level in the traj-GEOSCCM run is close to that from the traj-ERAi run (solid line with circular marker, Fig. 3.14a). During the period 2089 to 2098, the traj-GEOSCCM run predicts there will be little change in the FDP levels throughout the year (dashed line with circular marker). We notice there's a slight increase in the potential-temperature level of FDP in Fig. 3.14a. Since the predicted pressure levels of the FDPs in the traj-GEOSCCM run show little change (not shown), we conclude that the slight increase in the potential-temperature level of FDP is mainly due to an increase in temperature (Fig.3.14b) rather than a decrease in pressure, which is consistent with our result in Fig. 3.13a.

The traj-WACCM run produces much higher FDP levels in winter (solid line with triangular marker, Fig. 3.14a) during the period 2005 to 2014, and predicts that the FDP level will increase significantly by the end of the century (dashed line with triangular marker). The elevated FDP level in the traj-WACCM run is in agreement with its latitude-altitude

distribution of changes in the FDPs and the intense increase in the temperatures near the coldest levels in the TTL (Figures. 3.13b and 3.14b). The intense increase in the TTL temperature may be attributed to the RCP 8.5 scenario that drives the WACCM, which produces a warm bias in the coldest regions [Kim et al., 2013]. However, the seasonal cycle of the FDP level predicted by the traj-WACCM run will become weaker. The weakened seasonal cycle of the TTL temperature (Fig. 3.14b) together with the weakened seasonal cycle of FDP level result in the smaller amplitude of the seasonal cycle of the tropical lower stratospheric water vapor by the end of the 21st century as predicted by the WACCM (Fig. 3.11).

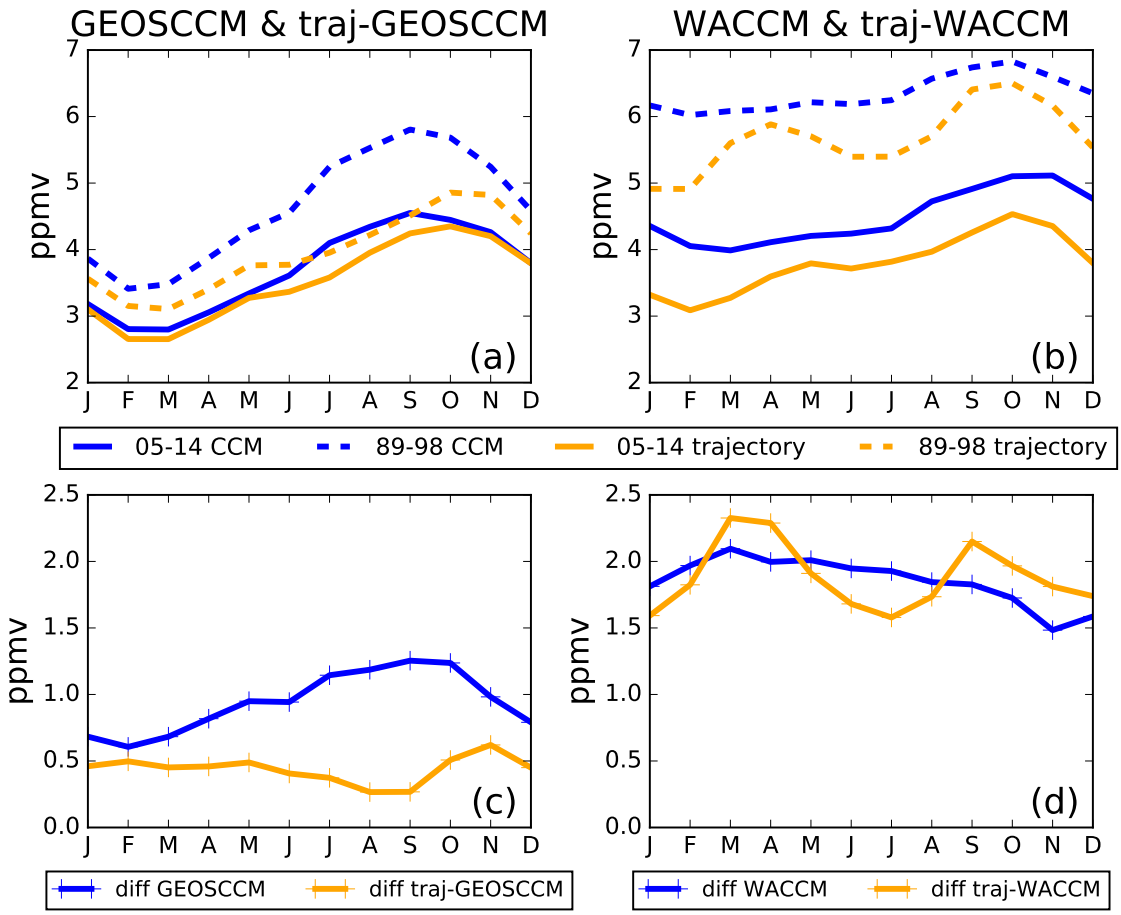

Figure 3.11: Panels (a) and (b): Comparison between the seasonal cycle (ppmv) of the tropical lower stratospheric water vapor averaged over the period 2005 to 2014 and the seasonal cycle averaged over the period 2089 to 2098 in the CCMs and the trajectory model driven by the CCMs. Panels (c) and (d): the difference (ppmv) between seasonal cycles during 2089 - 2098 and the seasonal cycles during 2005 - 2014.

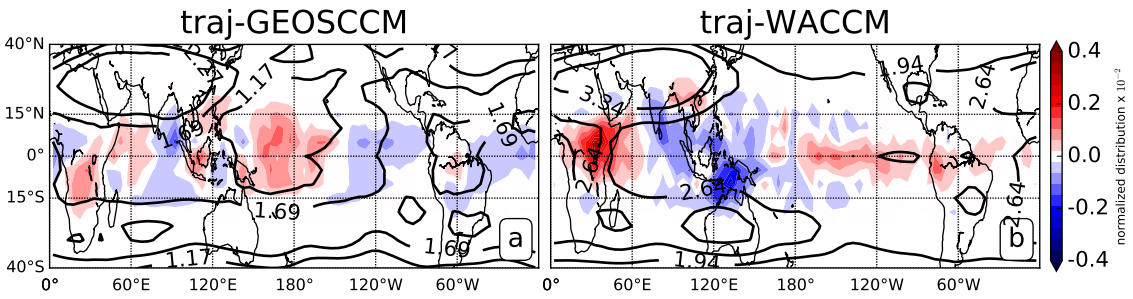

Figure 3.12: The annual average horizontal distribution of changes in the FDPs (normalized distribution $\times 10^{-2}$) by the end of the 21st century. The change in the FDPs is obtained by differencing the FDP distribution during 2089 - 2098 and the FDP distribution during 2005 - 2014. (a) traj-GEOSCCM run and (b) traj-WACCM run. The black contour shows the changes in the temperatures at the coldest levels. The coldest levels are found in the annual average zonal mean temperature fields during 2005 to 2014 shown in Fig.3.13, which is 360 K - 400 K potential temperatures in the GEOSCCM and 360 K - 420 K potential temperatures in the WACCM.

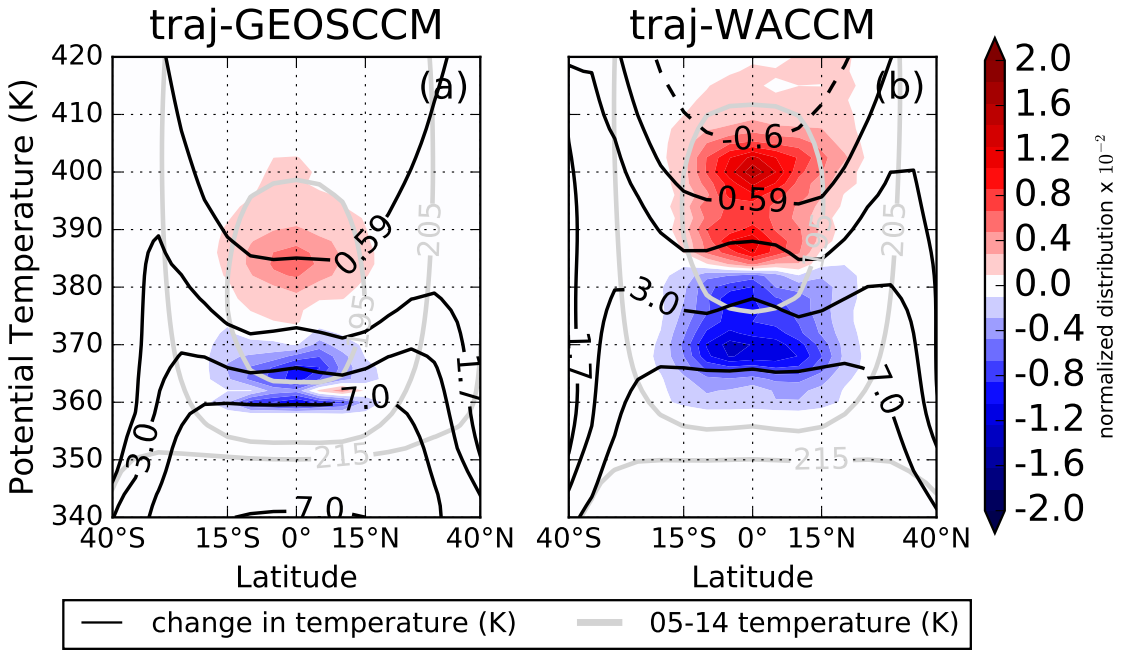

Figure 3.13: The annual average vertical distribution of changes in the FDPs (normalized distribution $\times 10^{-2}$) by the end of the 21st century predicted by (a) traj-GEOSCCM run and (b) traj-WACCM run, with the differences of the zonal mean temperatures between periods 2089-2098 and 2005-2014 (black) and the 2005-2014 zonal mean temperature field (gray) over-plotted.

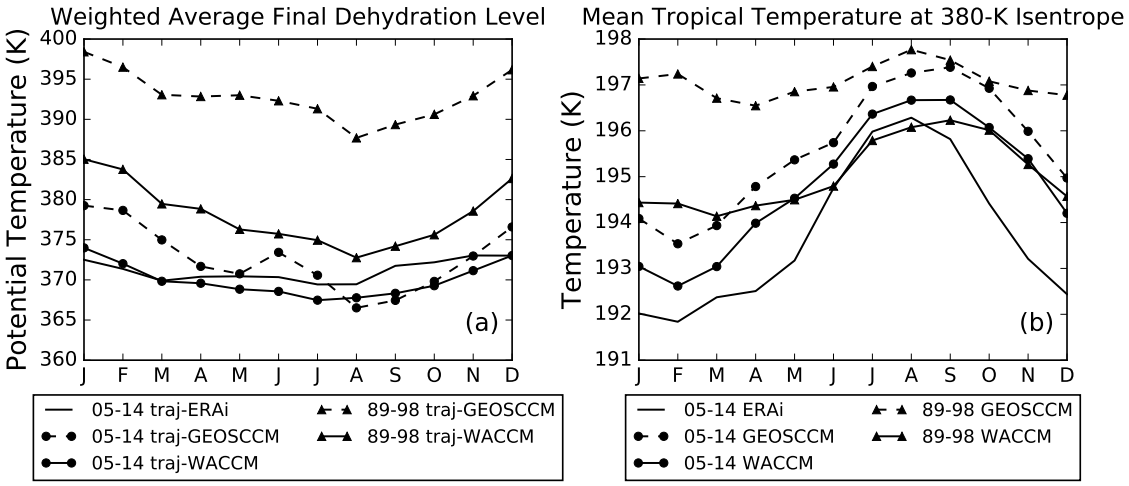

Figure 3.14: (a) Annual cycle of weighted average FDP level (potential temperature, K), which is the average isentropic level when weighted by the number of FDPs at each level. (b) Annual cycle of temperature (K) averaged at the 380-K surface between $\pm$ 20 ° latitudes.

IV SUMMARY

In this study, we evaluate how well two state-of-the-art chemistry-climate models (CCMs) reproduce the observed seasonal cycle of the tropical lower stratospheric water vapor. The chemistry-climate models include the Goddard Earth Observing System Chemistry Climate Model (GEOSCCM) and the Whole Atmosphere Community Climate Model (WACCM). We do this by comparing the seasonal cycle of the tropical lower stratospheric water vapor between the CCMs and the observations. We also evaluate the key processes that regulate the tropical lower stratospheric water vapor using a forward, domain filling, diabatic trajectory model. Furthermore, we explore how the seasonal cycle of the tropical lower stratospheric water vapor changes over the 21st century in the CCMs.

We first compare the tropical lower stratospheric water vapor from the two CCMs with that from the Earth Observing System (EOS) Microwave Limb Sounder (MLS) and that from European Centre for Medium-Range Weather Forecasts (ECMWF) ERA-Interim (ERAi) during the period 2005 to 2014. We show the seasonal cycle of the 100-hPa water vapor mixing ratio (ppmv) averaged between 20°S - 20°N latitudes (Fig. 3.1), the horizontal distribution of 100-hPa water vapor (Fig. 3.2), and the water vapor mass flux across the 100-hPa surface (Fig. 3.4).

The seasonal cycle from the GEOSCCM is overall in good agreement with that from the MLS and the ERAi. But the horizontal distribution of 100-hPa water vapor in the GEOSCCM shows differences. During boreal summer (JJA), the GEOSCCM overesti-

mates the water vapor concentration in the Subtropical West Pacific and underestimates the water vapor concentration in the deep tropics (15°S - 15°N) and the southern hemisphere.

The WACCM overall produces a higher water vapor concentration in both the seasonal cycle and the 100-hPa horizontal distributions. In the 100-hPa horizontal distribution, the boreal winter (DJF) water vapor concentration is especially large, which is on average 1.29 ppmv and 1.02 ppmv larger than that in the MLS and in the ERAi respectively. This results in a weaker seasonal contrast in both the horizontal distributions and the seasonal cycle in the WACCM.

The water vapor mass flux (Fig. 3.4) in the ERAi shows that strong upward transport of water vapor into the stratosphere locates in the deep tropics (15°S - 15°N), especially the Tropical West Pacific, throughout the year. Other flux maxima locate in the Asian monsoon region during summer and in South America during winter. These regions of stronger upward transport also correspond to the regions of stronger upward motion (Fig. 3.3), which suggests that the upward motion through the tropopause plays a more important role than the spatial variability of the 100-hPa water vapor concentration in controlling the water vapor mass flux through the 100-hPa surface.

The water vapor mass flux in the GEOSCCM shows a similar pattern with that in the ERAi, but with smaller intensity, which can be explained by the weaker upward motion (Fig. 3.3) in the GEOSCCM. The overestimation of the JJA water vapor concentration in the Subtropical West Pacific results in an overestimation of the dominance of the upward

transport in that region during summer and an underestimation of the dominance in the Tropical West Pacific. The WACCM shows a much more localized pattern of the upward transport, which is confined in the Tropical West Pacific throughout the year.

We then evaluate the mechanisms underlying the seasonal cycle of the tropical lower stratospheric water vapor using the trajectory model. The trajectory model is driven by two dimensional horizontal winds, diabatic heating rates, and temperatures from the ERAi (traj-ERAi), GEOSCCM (traj-GEOSCCM), and WACCM (traj-WACCM). The seasonal cycle of the tropical lower stratospheric water vapor in the trajectory model is defined to be the monthly water vapor mixing ratio (ppmv) averaged between 20°S - 20°N over the period 2005 to 2014 at latitudes and 380 K - 390 K potential temperatures.

We validate the seasonal cycles simulated by the trajectory model compared to the observation and the CCMs. The trajectory model shows differences in the water vapor concentration in the seasonal cycle. Since we didn't include adjustments for cloud physics [Jensen et al., 2001] or the moistening effect of anvil ice from convective overshooting [e.g. Dessler, 2002; Jensen et al., 2007; Dessler et al., 2007] in our trajectory model, it results in an underestimation of the water vapor concentration in the seasonal cycle compared to the observation [Schoeberl et al., 2014]. However, the trajectory model shows little bias in the phase and amplitude of the seasonal cycle. The agreement in the seasonal oscillation of the annual cycles between the trajectory model, the MLS, and the CCMs indicates that the seasonal variability is largely controlled by the TTL temperatures. The agreement also suggests that the trajectory model can be an adequate tool to evaluate the key processes

regulating the seasonal cycle of the tropical lower stratospheric water vapor in the CCMs.

We next examine the details of the transport of water vapor into the stratosphere in the trajectory model. We use the contribution to $m_{H_2O}^{entry}$ from the 360-K level (Fig. 3.6), where the notation $m_{H_2O}^{entry}$ indicates the mass of water vapor entering the stratosphere. The traj-ERAi run shows that the contribution from the deep tropics (15°S - 15°N) is strong throughout the year, and that the contributions from the subtropics show seasonal variability. In boreal summer, regions of strong contribution include the Asian monsoon region, Subtropical West Pacific, Tropical West Pacific, and East Pacific. While in boreal winter, more water vapor originates from Tropical Africa, Tropical West Pacific, northern Australia, and Tropical America. The differences between the contribution to $m_{H_2O}^{entry}$ from the 360-K level and the water vapor mass flux at the 100-Pa level indicates moisture is horizontally transported during its journey upward into the stratosphere, which agrees with previous studies that emphasized the importance of horizontal movement while air parcels are transported upward into the stratosphere [e.g. Holton and Gettelman, 2001; Fueglistaler et al., 2004; Bonazzola and Haynes, 2004; Levine et al., 2007].

The traj-GEOSCCM run does a good job reproducing the contribution to $m_{H_2O}^{entry}$ from the 360-K level, but it shows general underestimation compared to the traj-ERAi run. The traj-WACCM run shows larger differences, including an overestimation in the contribution from the Tropical West Pacific during both summer and winter. The traj-WACCM run also underestimates the contribution from all other regions. This suggests that the two dimensional horizontal winds and diabatic heating rates from the WACCM that drive the

parcel trajectories need improvement.

Since TTL temperatures largely control the seasonal cycle of the stratospheric water vapor, it is necessary that we examine how well the GEOSCCM and WACCM reproduce where parcels in the trajectory model encounter the region of lowest temperatures and reach the final dehydration point (FDP) during 2005 to 2014 (Figures 3.7 and 3.8). The traj-ERAi run shows that most FDPs take place in between 15°S and 15°N, where the troposphere-to-stratosphere transport of water vapor is strong (Figures 3.4 and 3.6) and the temperatures are low [Fueglistaler et al., 2009]. In this latitude range, the JJA FDP maxima occur in South Asia and the Tropical Pacific, while the DJF FDP maxima occur in the Tropical West Pacific, Tropical Africa, and South America.

The traj-GEOSCCM run underestimates the dominance of FDPs in South Asia. While the traj-WACCM run shows substantial overestimation in the winter FDP density in southern Tropical West Pacific. The traj-WACCM run also underestimates the winter FDP density in Tropical Africa and Tropical America. These differences in the FDP patterns from the traj-GEOSCCM and traj-WACCM are attributed to the differences in the details of the transport patterns they produced (Figures 3.4 and 3.6).

The vertical distribution of FDPs in the traj-GEOSCCM run agrees with the traj-ERAi run that most of the FDPs take place below the 380-K potential temperature surface in the coldest region in the TTL (Fig. 3.8). However, the traj-WACCM run shows that the FDPs locate at higher levels than those in the traj-ERAi run. Specifically, 33% of the parcels in the traj-WACCM run dehydrate above the 380-K surface (Table 2.1). This occurs

because the coldest region in the WACCM is centered at a higher altitude than that in the ERAi.

We then further investigate how well the CCMs reproduce the contribution to the seasonal cycle of the tropical lower stratospheric water vapor from the three latitude bands: 40°S - 15°S (SH), 15°S - 15°N (TR), and 15°N - 40°N (NH) (Figures 3.9 and 3.10). Both the traj-GEOSCCM run and traj-WACCM run agree with the traj-ERAi run that water vapor originating from and entering the stratosphere in the TR largely controls the moisture, phase and the seasonal oscillation of the seasonal cycle. This is consistent with our result that the deep tropics (15°S - 15°N) dominates both the troposphere-to-stratosphere transport of water vapor (Figures 3.4 and 3.6) and the final dehydration (Fig. 3.7) throughout the year. The traj-GEOSCCM run and traj-WACCM run also agree with the traj-ERAi run that the NH contributes a smaller part of the seasonal cycle and that the SH makes almost no contribution.

Finally, we examine how the seasonal cycle of the tropical lower stratospheric water vapor changes during the 21st century in the two CCMs (Fig. 3.11). Both the GEOSCCM and the WACCM predict the seasonal cycle will be moister throughout the year by the end of the century. The mean of the seasonal cycle will increase by 0.93 ppmv (25%) in the GEOSCCM and 1.85 ppmv (41%) in the WACCM (Table 3.1). This is consistent with the increase of the temperature at the 380-K surface during the century predicted by the two CCMs (Fig. 3.14b). However, the two CCMs disagree with the change in the amplitude of the seasonal cycle during the century. The GEOSCCM predicts the amplitude will increase

by 0.64 ppmv (36%), while the WACCM predicts the amplitude will decrease by 0.32 ppmv (28%).

In the meantime, we also test if the trajectory model driven by the CCMs does a good job reproducing those changes. The trajectory runs agree with the CCMs that the water vapor concentration in the seasonal cycle will be increasing during the 21st century. However, both the traj-GEOSCCM and traj-WACCM runs under predict the changes in the water vapor concentration and failed to show changes in the amplitude of the seasonal cycle. Since we didn't include the evaporation of lofted ice in our trajectory runs, the impact of the long-term changes in the evaporation of lofted ice, which play important roles in the changes of the tropical lower stratosphere moisture for the two CCMs [Dessler et al., 2016], is missing in our trajectory results. The changes in both the mean value and the amplitude of the seasonal cycle are better reproduced if ice data from the GEOSCCM and WACCM is added to the trajectory model (not shown).

Since the long-term trend of the TTL temperatures largely controls the changes in the stratospheric water vapor during the 21st century [e.g. Fueglistaler and Haynes, 2005; Oman et al., 2008; Gettelman et al., 2009; Kim et al., 2013], and that most FDPs occur at the coldest levels in the TTL, it is necessary for us to investigate how the FDP locations change in the trajectory model driven by the CCMs as the climate warms. In general, both the traj-GEOSCCM run and traj-WACCM run show that the changes in the TTL temperatures and the altitude of the coldest region will largely control the FDP pattern both vertically and horizontally (Figures 3.12, 3.13, and 3.14).

The annual average horizontal distributions of the changes in the FDPs from the traj-GEOSCCM run and traj-WACCM run show different patterns (Fig. 3.12). The disagreement comes from the different patterns shown in the changes of the temperatures at the coldest levels in the GEOSCCM and the WACCM. The traj-GEOSCCM run shows that the FDPs will increase in the Tropical West Pacific, where the increase in the temperatures is the smallest. While the decrease of the FDPs occurs in other regions outside of the Tropical West Pacific, where the temperatures will increase more intensely. The traj-WACCM run, however, shows the FDPs will decrease in the Indian Ocean, the Indonesian region, and northern Australia. The decrease of the FDPs in the traj-WACCM run is co-located with a maximum increase in the temperatures at the coldest levels.

There are also differences in the vertical distribution of the changes in the FDPs between the traj-GEOSCCM run and the traj-WACCM run (Fig. 3.13). In the traj-GEOSCCM run, there is an increase in the FDPs at the upper center of the coldest levels in the TTL (375 K - 400 K potential temperature), while the decrease in the FDPs will occur around the lower levels of the coldest region (360 K - 370 K potential temperature). But overall there's little change in the average FDP level in the traj-GEOSCCM run (Fig. 3.14a). The traj-WACCM run, on the other hand, predicts the FDPs will rise significantly, with increasing FDPs reaching as high as $\sim$420-K potential temperature. This corresponds to a more significant increase in the TTL temperatures (Fig. 3.14b) and a rise of the coldest levels in the TTL during the century.

REFERENCES

Bannister, R., O'neill, A., Gregory, A., and Nissen, K., 2004: The role of the south-east asian monsoon and other seasonal features in creating the tape-recorder signal in the unified model. *Quarterly Journal of the Royal Meteorological Society*, **130 (599)**, 1531–1554, doi:10.1256/qj.03.106.

Bates, D. R. and Nicolet, M., 1950: The photochemistry of atmospheric water vapor. *Journal of Geophysical Research*, **55 (3)**, 301–327, doi:10.1029/JZ055i003p00301.

Bergman, J. W., Fierli, F., Jensen, E. J., Honomichl, S., and Pan, L. L., 2013: Boundary layer sources for the asian anticyclone: Regional contributions to a vertical conduit. *Journal of Geophysical Research: Atmospheres*, **118 (6)**, 2560–2575, doi:10.1002/jgrd.50142.

Bonazzola, M. and Haynes, P., 2004: A trajectory-based study of the tropical tropopause region. *Journal of Geophysical Research: Atmospheres*, **109 (D20)**, doi:10.1029/2003JD004356.

Bowman, K. P., 1993: Large-scale isentropic mixing properties of the antarctic polar vortex from analyzed winds. *Journal of Geophysical Research: Atmospheres*, **98 (D12)**, 23 013–23 027, doi:10.1029/93JD02599.

Bowman, K. P. and Carrie, G. D., 2002: The mean-meridional transport circulation of the

troposphere in an idealized gcm. *Journal of the atmospheric sciences*, **59 (9)**, 1502–1514, doi:10.1175/1520-0469(2002)059<1502:TMMTCO>2.0.CO;2.

Brewer, A., 1949: Evidence for a world circulation provided by the measurements of helium and water vapour distribution in the stratosphere. *Quarterly Journal of the Royal Meteorological Society*, **75 (326)**, 351–363, doi:10.1002/qj.49707532603.

Dee, D., Uppala, S., Simmons, A., Berrisford, P., Poli, P., Kobayashi, S., Andrae, U., Balmaseda, M., Balsamo, G., Bauer, P., et al., 2011: The era-interim reanalysis: Configuration and performance of the data assimilation system. *Quarterly Journal of the royal meteorological society*, **137 (656)**, 553–597, doi:10.1002/qj.828.

Dessler, A., 1998: A reexamination of the stratospheric fountain hypothesis. *Geophysical Research Letters*, **25 (22)**, 4165–4168, doi:10.1029/1998GL900120.

Dessler, A., 2002: The effect of deep, tropical convection on the tropical tropopause layer. *Journal of Geophysical Research: Atmospheres*, **107 (D3)**, ACH 6–1–ACH 6–5, doi:10.1029/2001JD000511.

Dessler, A., Hanisco, T., and Fueglistaler, S., 2007: Effects of convective ice lofting on h2o and hdo in the tropical tropopause layer. *Journal of Geophysical Research: Atmospheres*, **112 (D18)**, n/a–n/a, doi:10.1029/2007JD008609.

Dessler, A., Schoeberl, M., Wang, T., Davis, S., and Rosenlof, K., 2013: Stratospheric water vapor feedback. *Proceedings of the National Academy of Sciences*, **110 (45)**, 18 087–18 091, doi:10.1073/pnas.1310344110.

Dessler, A., Weinstock, E. M., Hintsa, E., Anderson, J., Webster, C., May, R., Elkins, J., and Dutton, G., 1994: An examination of the total hydrogen budget of the lower stratosphere. *Geophysical research letters*, **21 (23)**, 2563–2566, doi:10.1029/94GL02283.

Dessler, A., Ye, H., Wang, T., Schoeberl, M., Oman, L., Douglass, A., Butler, A., Rosenlof, K., Davis, S., and Portmann, R., 2016: Transport of ice into the stratosphere and the humidification of the stratosphere over the 21st century. *Geophysical Research Letters*, **43 (5)**, 2323–2329, doi:10.1002/2016GL067991.

Dvortsov, V. L. and Solomon, S., 2001: Response of the stratospheric temperatures and ozone to past and future increases in stratospheric humidity. *Journal of Geophysical Research: Atmospheres*, **106 (D7)**, 7505–7514, doi:10.1029/2000JD900637.

Forster, P. M. d. F. and Shine, K. P., 1999: Stratospheric water vapour changes as a possible contributor to observed stratospheric cooling. *Geophysical Research Letters*, **26 (21)**, 3309–3312, doi:10.1029/1999GL010487.

Forster, P. M. d. F. and Shine, K. P., 2002: Assessing the climate impact of trends in stratospheric water vapor. *Geophysical Research Letters*, **29 (6)**, 10–1–10–4, doi: 10.1029/2001GL013909.

Fueglistaler, S., Bonazzola, M., Haynes, P., and Peter, T., 2005: Stratospheric water vapor predicted from the lagrangian temperature history of air entering the stratosphere in the tropics. *Journal of Geophysical Research: Atmospheres*, **110 (D8)**, doi: 10.1029/2004JD005516.

Fueglistaler, S., Dessler, A., Dunkerton, T., Folkins, I., Fu, Q., and Mote, P. W., 2009: Tropical tropopause layer. *Review of Geophysics*, **47**, 1–31, doi:10.1029/2008RG000267.

Fueglistaler, S. and Haynes, P., 2005: Control of interannual and longer-term variability of stratospheric water vapor. *Journal of Geophysical Research: Atmospheres*, **110 (D24)**, doi:10.1029/2005JD006019.

Fueglistaler, S., Wernli, H., and Peter, T., 2004: Tropical troposphere-to-stratosphere transport inferred from trajectory calculations. *Journal of Geophysical Research: Atmospheres*, **109 (D3)**, 1–16, doi:10.1029/2003JD004069.

Garny, H. and Randel, W. J., 2016: Transport pathways from the asian monsoon anticyclone to the stratosphere. *Atmospheric Chemistry and Physics*, **16 (4)**, 2703–2718, doi:10.5194/acp-16-2703-2016.

Gettelman, A., Kinnison, D. E., Dunkerton, T. J., and Brasseur, G. P., 2004: Impact of monsoon circulations on the upper troposphere and lower stratosphere. *Journal of Geophysical Research: Atmospheres*, **109 (D22)**, doi:10.1029/2004JD004878.

Gettelman, A., Randel, W., Wu, F., and Massie, S., 2002: Transport of water vapor in the tropical tropopause layer. *Geophysical research letters*, **29 (1)**, 9–1–9–4, doi:10.1029/2001GL013818.

Gettelman, A., Birner, T., Eyring, V., Akiyoshi, H., Bekki, S., Brühl, C., Dameris, M.,

Kinnison, D., Lefèvre, F., and Lott, F., 2009: The tropical tropopause layer 1960–2100. *Atmospheric Chemistry and Physics*, **9 (5)**, 1621–1637, doi:10.5194/acp-9-1621-2009.

Gettelman, A., Hegglin, M. I., Son, S.-W., Kim, J., Fujiwara, M., Birner, T., Kremser, S., Rex, M., Añel, J., Akiyoshi, H., et al., 2010: Multimodel assessment of the upper troposphere and lower stratosphere: Tropics and global trends. *Journal of Geophysical Research: Atmospheres*, **115 (D3)**, n/a–n/a, doi:10.1029/2009JD013638.

Grosvenor, D., Choularton, T., Coe, H., and Held, G., 2007: A study of the effect of over-shooting deep convection on the water content of the ttl and lower stratosphere from cloud resolving model simulations. *Atmospheric Chemistry and Physics*, **7 (18)**, 4977–5002, doi:10.1029/1999JD901133.

Hatsushika, H. and Yamazaki, K., 2003: Stratospheric drain over indonesia and dehydration within the tropical tropopause layer diagnosed by air parcel trajectories. *Journal of Geophysical Research: Atmospheres*, **108 (D19)**, doi:10.1029/2002JD002986.

Holton, J. R. and Gettelman, A., 2001: Horizontal transport and the dehydration of the stratosphere. *Geophysical Research Letters*, **28 (14)**, 2799–2802, doi:10.1029/2001GL013148.

Hoskins, B. J., 1991: Towards a pv-θ view of the general circulation. *Tellus A: Dynamic Meteorology and Oceanography*, **43 (4)**, 27–35, doi:10.1034/j.1600-0870.1991.t01-3-00005.x.

Jensen, E. and Pfister, L., 2004: Transport and freeze-drying in the tropical tropopause layer. *Journal of Geophysical Research: Atmospheres*, **109 (D2)**, doi:10.1029/2003JD004022.

Jensen, E. J., Ackerman, A. S., and Smith, J. A., 2007: Can overshooting convection dehydrate the tropical tropopause layer? *Journal of Geophysical Research: Atmospheres*, **112 (D11)**, doi:10.1029/2006JD007943.

Jensen, E. J., Pfister, L., Ackerman, A. S., Tabazadeh, A., and Toon, O. B., 2001: A conceptual model of the dehydration of air due to freeze-drying by optically thin, laminar cirrus rising slowly across the tropical tropopause. *Journal of geophysical research*, **106 (17)**, 237–17, doi:10.1029/2000JD900649.

Kim, J., Grise, K. M., and Son, S.-W., 2013: Thermal characteristics of the cold-point tropopause region in cmip5 models. *Journal of Geophysical Research: Atmospheres*, **118 (16)**, 8827–8841, doi:10.1002/jgrd.50649.

Lelieveld, J., Brühl, C., Jockel, P., Steil, B., Crutzen, P., Fischer, H., Giorgetta, M., Hoor, P., Lawrence, M., Sausen, R., et al., 2007: Stratospheric dryness: model simulations and satellite observations. *Atmospheric Chemistry and Physics*, **7 (5)**, 1313–1332, doi:10.5194/acp-7-1313-2007.

Levine, J., Braesicke, P., Harris, N., Savage, N., and Pyle, J., 2007: Pathways and timescales for troposphere-to-stratosphere transport via the tropical tropopause layer and

their relevance for very short lived substances. *Journal of Geophysical Research: Atmospheres*, **112 (D4)**, 1–15, doi:10.1029/2005JD006940.

Marsh, D. R., Mills, M. J., Kinnison, D. E., Lamarque, J.-F., Calvo, N., and Polvani, L. M., 2013: Climate change from 1850 to 2005 simulated in cesm1 (waccm). *Journal of climate*, **26 (19)**, 7372–7391, doi:10.1175/JCLI-D-12-00558.1.

Maycock, A. C., Joshi, M. M., Shine, K. P., and Scaife, A. A., 2013: The circulation response to idealized changes in stratospheric water vapor. *Journal of Climate*, **26 (2)**, 545–561, doi:10.1175/JCLI-D-12-00155.1.

Molod, A., Takacs, L., Suarez, M., Bacmeister, J., Song, I.-S., and Eichmann, A., 2012: The geos-5 atmospheric general circulation model: Mean climate and development from merra to fortuna. Tech. rep., NASA/TM-2012-104606.

Mote, P. W., Rosenloh, K. H., Holton, J. R., Harwood, R. S., and Waters, J. W., 1995: Seasonal variations of water vapor in the tropical lower stratosphere. *Geophysical Research Letters*, **22 (9)**, 1093–1096, doi:10.1029/95GL01234.

Mote, P. W., Rosenlof, K. H., McIntyre, M. E., Carr, E. S., Gille, J. C., Holton, J. R., Kinnersley, J. S., Pumphrey, H. C., Russell III, J. M., and Waters, J. W., 1996: An atmospheric tape recorder: The imprint of tropical tropopause temperatures on stratospheric water vapor. *Journal of Geophysical Research*, **101 (D2)**, 3989–4006, doi:10.1029/95JD03422.

Newell, R. E. and Gould-Stewart, S., 1981: A stratospheric fountain? *Journal of Atmospheric Science*, **38 (12)**, 2789–2796, doi:10.1175/1520-0469(1981)038<2789:ASF>2.0.CO;2.

Oman, L., Waugh, D. W., Pawson, S., Stolarski, R. S., and Nielsen, J. E., 2008: Understanding the changes of stratospheric water vapor in coupled chemistry-climate model simulations. *Journal of the Atmospheric Sciences*, **65 (10)**, 3278–3291, doi:10.1175/2008JAS2696.1.

Orbe, C., Waugh, D. W., and Newman, P. A., 2015: Air-mass origin in the tropical lower stratosphere: The influence of asian boundary layer air. *Geophysical Research Letters*, **42 (10)**, 4240–4248, doi:10.1002/2015GL063937.

Park, M., Randel, W. J., Kinnison, D. E., Garcia, R. R., and Choi, W., 2004: Seasonal variation of methane, water vapor, and nitrogen oxides near the tropopause: Satellite observations and model simulations. *Journal of Geophysical Research: Atmospheres*, **109 (D3)**, doi:10.1029/2003JD003706.

Pumphrey, H. C., Clark, H. L., and Harwood, R. S., 2000: Lower stratospheric water vapor measured by uars mls. *Geophysical research letters*, **27 (12)**, 1691–1694, doi:10.1029/1999GL011339.

Randel, W. J., Wu, F., Gettelman, A., Russell III, J. M., Zawodny, J. M., and Oltmans, S. J., 2001: Seasonal variation of water vapor in the lower stratosphere observed in halogen

occultation experiment data. *Journal of geophysical research*, **106 (D13)**, 14–313, doi: 10.1029/2001JD900048.

Randel, W. J., Wu, F., Oltmans, S. J., Rosenlof, K., and Nedoluha, G. E., 2004: Interannual changes of stratospheric water vapor and correlations with tropical tropopause temperatures. *Journal of the Atmospheric Sciences*, **61 (17)**, 2133–2148, doi:10.1175/1520-0469(2004)061<2133:ICOSWV>2.0.CO;2.

Randel, W. J., Wu, F., Russell III, J. M., Roche, A., and Waters, J. W., 1998: Seasonal cycles and qbo variations in stratospheric ch4 and h2o observed in uars haloe data. *Journal of the atmospheric sciences*, **55 (2)**, 163–185, doi:10.1175/1520-0469(1998)055<0163:SCAQVI>2.0.CO;2.

Rienecker, M., Suarez, M., Todling, R., Bacmeister, J., Takacs, L., Liu, H.-C., Gu, W., Sienkiewicz, M., Koster, R., Gelaro, R., et al., 2008: The geos-5 data assimilation system-documentation of versions 5.0. 1, 5.1. 0, and 5.2. 0. Tech. rep., NASA/TM.

Schoeberl, M. and Dessler, A., 2011: Dehydration of the stratosphere. *Atmospheric Chemistry and Physics*, **11 (16)**, 8433–8446, doi:10.5194/acp-11-8433-2011.

Schoeberl, M., Dessler, A., and Wang, T., 2013: Modeling upper tropospheric and lower stratospheric water vapor anomalies. *Atmospheric Chemistry and Physics*, **13 (15)**, 7783–7793, doi:10.5194/acp-13-7783-2013.

Schoeberl, M., Dessler, A., Wang, T., Avery, M. A., and Jensen, E. J., 2014: Cloud forma-

tion, convection, and stratospheric dehydration. *Earth and Space Science*, **1 (1)**, 1–17, doi:10.1002/2014EA000014.

Schoeberl, M. R., Jensen, E. J., and Woods, S., 2015: Gravity waves amplify upper tropospheric dehydration by clouds. *Earth and Space Science*, **2 (12)**, 485–500, doi: 10.1002/2015EA000127.

Sherwood, S. C. and Dessler, A., 2000: On the control of stratospheric humidity. *Geophysical research letters*, **27 (16)**, 2513–2516, doi:10.1029/2000GL011438.

Shindell, D. T., 2001: Climate and ozone response to increased stratospheric water vapor. *Geophysical Research Letters*, **28 (8)**, 1551–1554, doi:10.1029/1999GL011197.

Smith, C. A., Toumi, R., and Haigh, J. D., 2000: Seasonal trends in stratospheric water vapour. *Geophysical research letters*, **27 (12)**, 1687–1690, doi:10.1029/1999GL011160.

Solomon, S., Garcia, R. R., Rowland, F. S., and Wuebbles, D. J., 1986: On the depletion of antarctic ozone. *Nature*, **321 (6072)**, 755–758, doi:doi:10.1038/321755a0.

Solomon, S., Rosenlof, K. H., Portmann, R. W., Daniel, J. S., Davis, S. M., Sanford, T. J., and Plattner, G.-K., 2010: Contributions of stratospheric water vapor to decadal changes in the rate of global warming. *Science*, **327 (5970)**, 1219–1223, doi:10.1126/science. 1182488.

Van Vuuren, D. P., Edmonds, J., Kainuma, M., Riahi, K., Thomson, A., Hibbard, K., Hurtt,

G. C., Kram, T., Krey, V., Lamarque, J.-F., et al., 2011: The representative concentration pathways: an overview. *Climatic change*, **109**, 5–31, doi:10.1007/s10584-011-0148-z.

World Meteorological Organization, 2011: Scientific assessment of ozone depletion: 2010. **(52)**, Geneva, Switzerland.

Wright, J., Fu, R., Fueglistaler, S., Liu, Y., and Zhang, Y., 2011: The influence of summer-time convection over southeast asia on water vapor in the tropical stratosphere. *Journal of Geophysical Research: Atmospheres*, **116 (D12)**, 1–12, doi:10.1029/2010JD015416.